DEPARTMENT OF
MECHANICAL AND INDUSTRIAL
ENGINEERING

PEDRO MIGUEL MARTINS BOTELHO
BSc in ⟨Mechanical Engineering Sciences⟩

CONTROL AND OPTIMIZATION OF HIGH-PRESSURE COMPRESSOR BLADE DIMENSIONS AND CLEARANCES

INTRODUÇÃO À DISSERTAÇÃO

MASTER IN MECHANICAL ENGINEERING

NOVA University Lisbon
⟨february⟩, ⟨2025⟩

DEPARTMENT OF
MECHANICAL AND INDUSTRIAL ENGINEER-
ING

CONTROL AND OPTIMIZATION OF HIGH-PRESSURE COMPRESSOR BLADE DIMENSIONS AND CLEARANCES

INTRODUÇÃO À DISSERTAÇÃO

PEDRO MIGUEL MARTINS BOTELHO

BSc in ⟨Mechanical Engineering Sciences⟩

Adviser: João Fradinho
Assistant Professor, NOVA University Lisbon

MASTER IN MECHANICAL ENGINEERING

NOVA University Lisbon
⟨february⟩, ⟨2025⟩

Control and Optimization of High-Pressure Compressor Blade Dimensions and Clearances

This document was created with the (pdf/Xe/Lua)LaTeX processor and the NOVAthesis template (v6.9.4) [9].

Contents

List of Figures

List of Tables

Acronyms

CAD Computer-Aided Design 20
CFMI CFM International 3
CL Chord Lenght 21
CMM Coordinate Measuring Machine 1, 20, 21, 29

FOD Foreign Object Damage 17

HP High Pressure 5, 9
HPC High Pressure Compressor v, 1, 9, 12–15, 18, 20, 23, 24
HPT High Pressure Turbine 9

LEAP Leading Edge Aviation Propulsion v, vii, 1, 3, 4, 6–8, 12–16, 24
LET Leading Edge Thickness 21
LP Low Pressure 5, 7–10
LPC Low Pressure Compressor 8, 9, 13
LPT Low Pressure Turbine v, 9, 10

ME Maintenance and Engineering 3, 19, 22, 25
MM Major Module 9
MRO Maintenance, Repair, and Overhaul 3

RTM Resin Transfer Molding 8

SB Service Bulletin 1

TAP Transportes Aéreos Portugueses vii, 1, 3, 6, 19, 22, 25, 30
TET Trailing Edge Thickness 21

1

Introduction

1.1 Motivation

In 2016, CFMI launched the LEAP-1A engine, ushering in a new era of efficiency and performance for commercial aviation. This engine builds on the solid foundation laid by the CFM56, which has been one of the most trusted and widely used engines in the industry.

Over the course of its life, an engine undergoes numerous upgrades and refinements aimed at improving its performance and fuel efficiency. These improvements often focus on precise measurements and dimensional control, as well as maintenance standards that ensure the engine continues to run smoothly and reliably. By implementing these updates, the engine can perform at its best throughout its service life, maximizing efficiency and reducing operational costs. Additionally, these advancements are aligned with the growing need for more sustainable aviation technologies, helping to meet the industry's environmental goals.

Each time an engine manufacturer introduces an optimization, it is implemented through a Service Bulletin (SB), a document that communicates details of modifications that can be made to the aircraft.

In recent years, two students, Edgar Farinhas and Pedro Rendas, explored a method for measuring the rotor blade dimensions of the HPC using a Coordinate Measuring Machine (CMM) machine, focusing specifically on the blades of the CFM56 HPC. [5]

Since it entered service, TAP has integrated the LEAP-1A into approximately half of its fleet, replacing the CFM56. As the performance of the HPC directly influences engine efficiency and overall operational effectiveness, establishing robust monitoring and control measures has become a critical priority, alongside investigating the factors that affect its performance.

1.2 Objectives

Various factors influence engine performance, and the high-pressure compressor (HPC) plays a key role in this. The efficiency of the HPC is largely determined by the design of its rotor blades, which operate under intense aerodynamic and thermal conditions. This directly impacts the engine's performance and fuel consumption. Despite their importance, TAP has no standardized dimensional inspection process for these components.

Using the available equipment at the TAP Engine Shop, including the 3D scanner and Coordinate Measuring Machine (CMM), this study aims to develop a practical and efficient method for measuring the chord length of HPC blades, as this parameter is crucial in assessing blade wear and its correlation with engine performance in test cell conditions. Additionally, the study seeks to create a tool to measure the total clearance of the entire stage after assembly, optimizing the assembly process and making it more efficient.

An important objective is to control the platform gap of the blades during their preparation for assembly, developing a tool capable of accurately simulating the blade fit. This will enable the immediate determination of the required number of wide and narrow platform blades, making the process faster and more efficient—an important consideration for TAP's operational needs.

By establishing this methodology, it will be possible to correlate these geometric characteristics with engine performance as tested in the test cell. Understanding these relationships will help optimize maintenance procedures and improve overall efficiency. This thesis represents an important step toward implementing a more advanced dimensional inspection process at TAP, contributing to the company's ongoing efforts to enhance engine performance and reliability.

2

Company and LEAP-1A Overview

2.1 TAP M&E

TAP was founded in 1945, during the end of World War II, a period marked by significant development in the aviation industry.

TAP Maintenance and Engineering (ME) is responsible for performing maintenance and engineering support services to TAP's airline fleet and third-party customers. Services such as Aircraft Maintenance, Engine Repair and Overhaul and Components Repair and Overhaul.

To maintain TAP Air Portugal's reputation as one of the most reliable airlines in the world, TAP ME embraces the concept of *Care2Quality*. This philosophy is founded on three key pillars: **Safety**, **Quality**, and **Relationships**. It is integrated across all TAP ME products and services, which are organized into five main departments: *Care2Airframe*, *Care2Engines*, *Care2Components*, *Care2Engineering*, and *Care2Technical Labs*.

TAP ME offers extensive Maintenance, Repair, and Overhaul (MRO) services for a variety of aircraft systems and engine models. For CFM International (CFMI) engines, including the CFM56 series and LEAP-1A, it provides light and heavy maintenance, engine testing, troubleshooting, redelivery checks, technical consulting, and engine trend monitoring.

Currently in its fleet TAP has the following aircraft:

Table 2.1: TAP Air Fleet Composition [3]

Aircraft	Active Nº	Age
Airbus A319ceo	3	23
Airbus A320ceo	15	19
Airbus A320neo	15	3
Airbus A321ceo	3	22
Airbus A321neo	12	4
Airbus A321LRneo	11	3
Airbus A330ceo	3	16
Airbus A330neo	19	5

2.2 LEAP Engine

LEAP engine family, developed and produced by CFM International—a joint venture between Safran Aircraft Engines and GE Aerospace—continues the legacy of the CFM56 as a best-seller in commercial aviation. Introduced in 2016, the LEAP powers the Airbus A320neo, Boeing 737 MAX, and COMAC C919, delivering a 15% improvement in fuel efficiency, along with reduced noise and emissions, while maintaining industry-leading reliability and cost-effectiveness. This advanced engine reflects the enduring success of the partnership between Safran and GE, which has been extended until 2050.

The LEAP, like most modern commercial aircraft engines, is a turbofan engine.

2.2.1 Turbofan

The Turbofan engine applies the same principle as the turbojet and all jet engines, Newton's third law: "For every action, there is an equal and opposite reaction". In this case, the first object is the engine itself and the second is the atmospheric air that is forced to accelerate as it passes through the engine causing the airplane to move forward.

To understand how the turbofan engine works, it is a good approach to analyze the turbojet working cycle and how it is processed first. As shown in Figure 2.1 the working cycle of a TurboJet has 4 main stages: Air intake, Compression, Combustion and Exhaust. At intake, the air is at atmospheric pressure, but as it passes through the compressors, it is compressed to optimal pressure and temperature conditions for combustion. Upon entering the combustion chamber, fuel nozzles mix the fuel and air, creating a homogeneous mixture that minimizes the peak temperature during combustion. During the combustion process, this mixture burns at constant pressure, increasing the air's volume while causing a decrease in pressure. The gases resulting from combustion expand through the turbine and jet pipe back to atmosphere providing the force needed to propel the airplane forward. During this part of the cycle, some of the energy in the expanding gases is turned into mechanical power by the turbine.

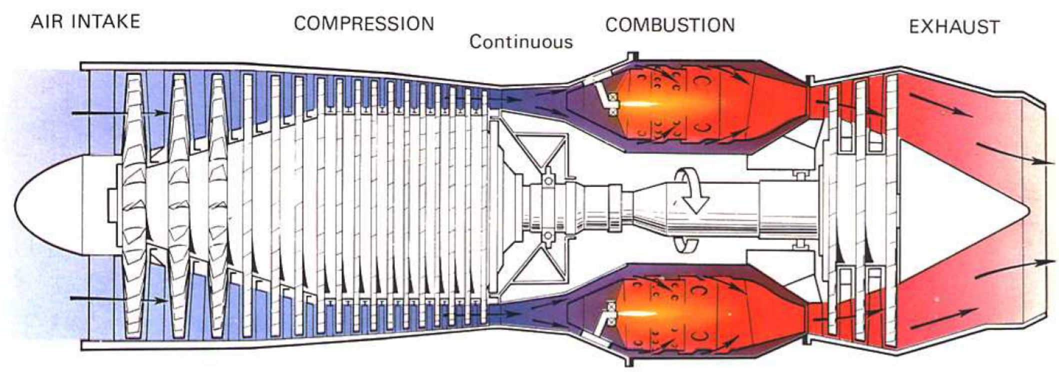

Figure 2.1: TurboJet Engine Work Cycle stages.[7]

Analysing the Turbofan work cycle requires a more complex approach since the air that goes through the combustor is now only responsible for 20% of the thrust power.

At the start, the engine's high-pressure shaft receives mechanical power with the assistance of a system called the Air Turbine Starter. This rotation drives the compressor blades, drawing air through the engine and initiating the compression process. The airflow through the engine also causes the fan to start moving. Once the engine reaches 20% of its maximum RPM, sufficient compression is generated to initiate combustion. With everything in motion, the engine enters a cycle similar to the turbojet working cycle. The gases produced from combustion expand through the High Pressure (HP) and Low Pressure (LP) turbines, delivering mechanical power to the HP and LP shafts. These shafts, in turn, transmit rotational energy to the HP and LP compressors as well as the front fan. As the fan rotates at high speed, it separates the incoming air into two distinct streams, forming the bypass ratio. Commercial aircraft engines, such as the LEAP-1A, are high-bypass ratio engines. In these engines, one stream of air enters the engine core, powering the turbojet-like working cycle. The remaining air, approximately 80% of the total intake, is channeled around the engine core. This bypassed air is directed into a narrow passage known as the fan duct, where its speed increases significantly. This accelerated airflow generates the majority of the thrust required to lift the aircraft.

In summary, the main differences between turbofan and turbojet engines lie in their airflow management and structural design. A key distinction is the large fan at the front of the turbofan, which directs a significant portion of the air around the engine core, defining the bypass ratio, which is the ratio of the amount of air bypassing the core to the amount of air passing through it, as illustrated in Figure 2.2. Wheight wise, for the same power output, given the fact that all the high pressure rotating assemblies diameter can be reduced, the turbofan engines are lighter, improving the power-wheight ratio of the engine. A low bypass ratio engine has a wheight reduction of 20 percent compared to a pure jet engine for the same air mass flow.[7] Another significant advancement in turbofan engines is the introduction of the multi-spool or multi-shaft system, although this technology can also be applied to pure jet engines. The presence of both LP and HP turbines and compressors requires each assembly to rotate at different speeds, since just a percentage of the air that flows through the LP Compressor goes into the HP one (the majority of the air forms the bypass flow). This is essential for achieving higher efficiency, as each component operates at its optimal rotational velocity. Most commercial aircraft engines are high-bypass engines, and the typical configuration for these engines is a two-shaft system. As illustrated in Figure 2.2 the LP compressor is powered by a shaft coming from the LP turbine, and the same applies to the HP spool.

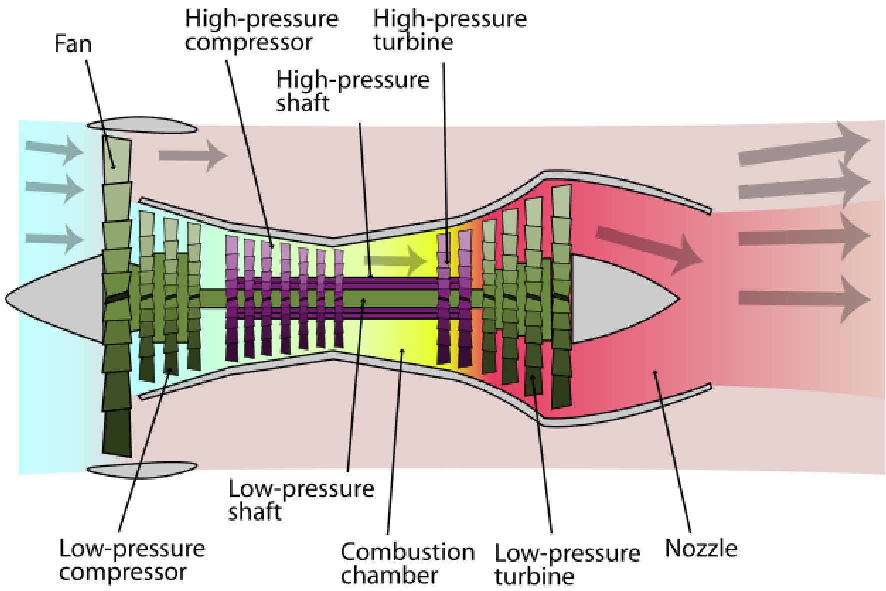

Figure 2.2: Turbofan Engine. [1]

2.2.2 LEAP Family

As mentioned at the beginning of this chapter, the LEAP engine powers a variety of aircraft, with its characteristics varying depending on the application. Therefore, we can categorize the LEAP engine family based on application and thrust power.

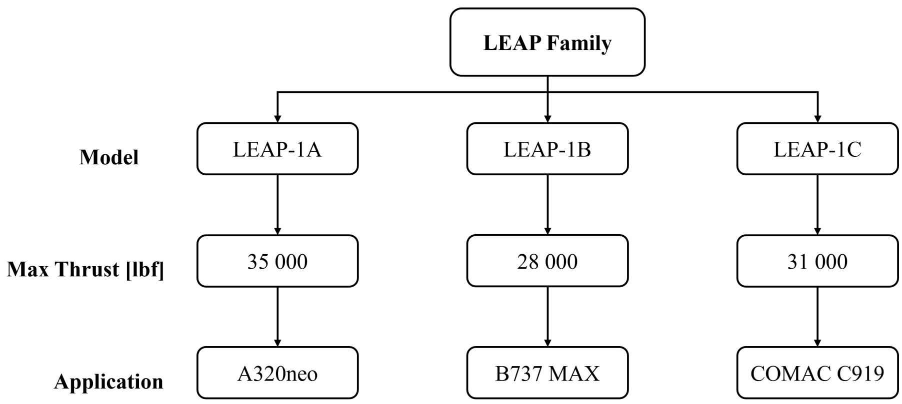

Figure 2.3: LEAP Family.[2]

Each model also has variations based on its thrust. For instance, the LEAP-1A can be further subcategorized into LEAP-1A23, LEAP-1A24, LEAP-1A26, LEAP-1A30, LEAP-1A32, LEAP-1A33, and LEAP-1A35. Considering that in 'LEAP-1A24', the '24' indicates the engine's thrust capacity of 24 klbf.

Currently, in the TAP Air Fleet Composition, the LEAP-1A26 and LEAP-1A32 engines are used respectively in the Airbus A320neo and A321neo.

2.2.3 LEAP-1A

The LEAP-1A, represented in Figure 2.4, is a high-bypass turbofan engine designed to power the next-generation Airbus A320neo. This section presents some of its key features, along with its main modules and innovations in comparison to its predecessor, the CFM56. Most of this information is derived from the engine's brochure and training manual.

Figure 2.4: LEAP-1A.[2]

This powerplant is presented with the following characteristics in Table 2.2.

Table 2.2: Characteristics of the LEAP-1A engine.[4]

Characteristic	**Value**
Takeoff thrust	Up to 35,000 lbf
Bypass ratio	11:1
Overall pressure ratio	40:1
Fan diameter	1.98 m (78 in)
Compressor stages (fan/booster/HPC)	1 + 3 + 10
Turbine stages (HP/LP)	2 + 7
Weight	3007 kg
Length	3.35 m (11 ft)
Width	2.53 m (8.3 ft)
Height	2.38 m (7.8 ft)

Design and function wise LEAP-1A present in its composition 4 Major modules. As represented in Figure 2.5, Fan and Booster, Core, LP Turbine and Accessory Drive Major Modules.

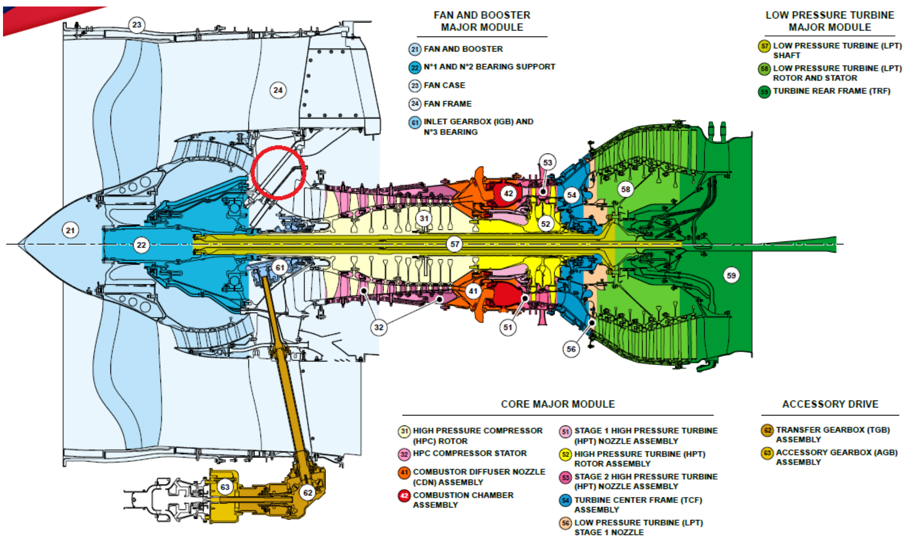

Figure 2.5: LEAP-1A Major Modules.[6]

2.2.3.1 Fan and Booster Major Module

As shown in Figure 2.5, the Fan and Booster Major Module consists of the Fan and Booster itself, two bearing supports, the fan case, the fan frame, the inlet gearbox, and the number 3 bearing.

The Fan and Booster assembly represents the integration of the front fan and the LP Compressor.

The fan itself is composed of a single assembly that includes one front spinner, 18 fan blades, a flow splitter, and a platform front shroud.

The Low Pressure Compressor (LPC) consists of three stages: the first stage has 62 blades, the second stage has 75 blades, and the third stage has 72 blades.

One of the major technological breakthroughs in the new LEAP-1A engine is the production of its fan blades. These blades are manufactured using additive manufacturing with 3D-woven Resin Transfer Molding (RTM) carbon fiber composites. Compared to the solid titanium blades of the CFM56, this advancement allows for larger blades, as illustrated in Figure 2.6, without increasing the engine's weight. According to the company, this material helps reduce engine weight by 500 lbs per unit.

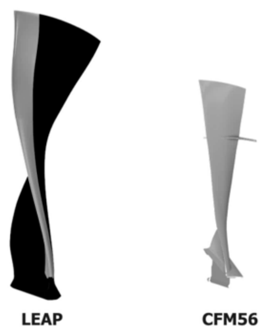

Figure 2.6: LEAP-1A fan blades vs CFM56 fan blades.[12]

In summary, the purpose of this engine assembly is to impart kinetic energy to the incoming airflow, separate the primary and secondary airflow, and expel the hot air generated by the engine.

2.2.3.2 Core

Next is the Core Major Module, which is responsible for generating thrust by producing power through highly compressed air.

This Major Module (MM) comprises the assembly of the HPC, combustion chamber, and High Pressure Turbine (HPT). Additionally, it is divided into nine sub-modules.

The HPC consists of the HPC rotor and stator, while the HPT includes the HPT rotor along with the stage 1 and stage 2 nozzle assemblies. The Core Major Module also incorporates the Turbine Center Frame and the LPT Stage 1 Nozzle.

To achieve optimal performance, the HPC features 10 stages, as shown in Table 2.3. Each stage consists of one rotor and one stator. The first five stages of compression are achieved through blisks, while the remaining five stages use compressor blades with circumferential assembly. This mini module has the purpose of increasing the pressure of the booster discharge air for combustion.

Table 2.3: Number of blades per stage on HPC [12]

Stage	1	2	3	4	5	6	7	8	9	10
Number of blades	-	-	-	-	-	62+2+2	57+2+2	63+2+2	60+2+2	64+2+2

It is important to note that the HPC rotor is coupled with the HPT, as shown in Figure 2.7. This coupling allows the kinetic energy extracted from the HPT to be used for compressing the airflow. Likewise, the same principle applies to the LPC and LPT.

In Figure 2.7, the yellow assembly represents the Low-Pressure rotor, while the orange assembly corresponds to the High-Pressure rotor.

As mentioned in 2.2.1, these rotors rotate at different speeds. The LP rotor operates at N1 speed (3 850 RPM), whereas the HP rotor rotates at N2 speed (16 645 RPM).

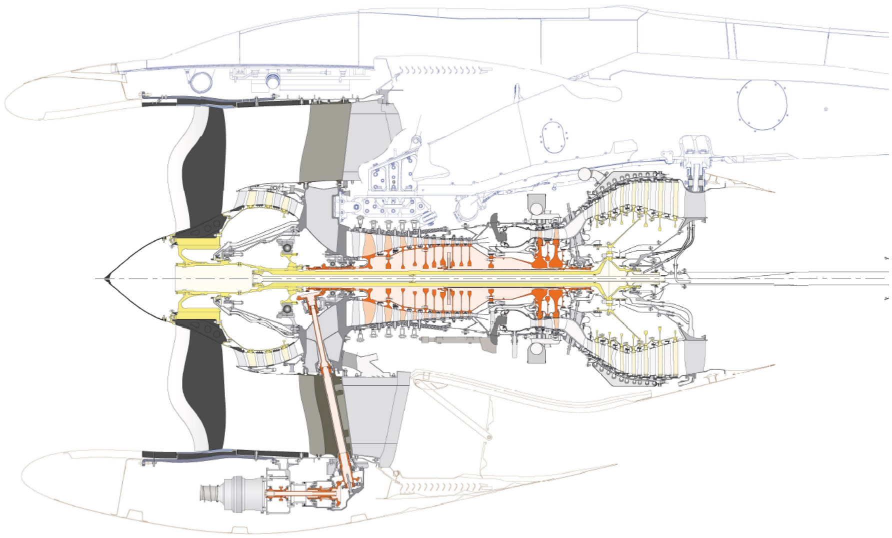

Figure 2.7: High and Low pressure rotors [12]

2.2.3.3 LP Turbine Major Module

The LP Turbine Major Module, represented in Figure 2.8, is composed by the LP turbine shaft, rotor and stator and the turbine rear frame.

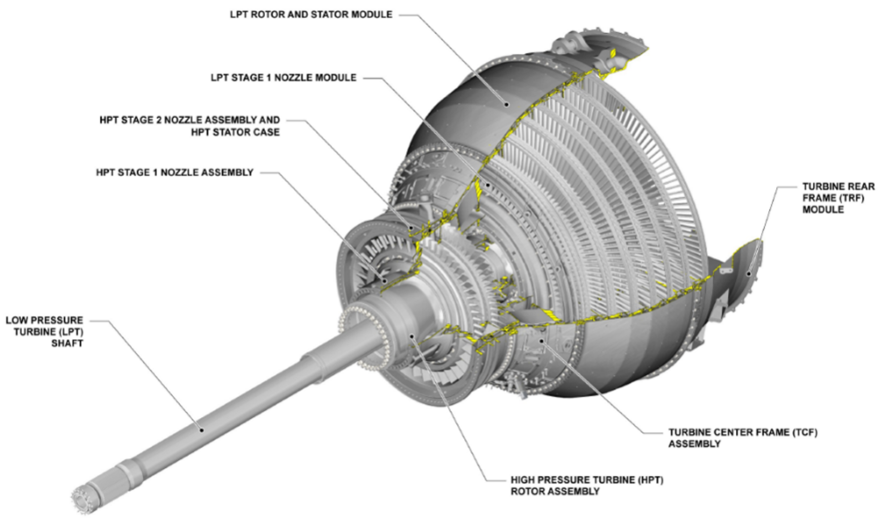

Figure 2.8: LPT. [12]

Its primary function is to supply mechanical power to the LP Compressor by converting the termal energy from the hot gases released from the combustion chambers into kinetic energy while simultaneously decompressing it.

It is worth noting that while both turbines and compressors present similar designs and compositions, their functions are fundamentally opposite.

As previously mentioned, compressors consume energy and transfer it to the air, compressing it while increasing its velocity, whereas turbines absorb energy from the expansion of the combustion gases and convert it into mechanical power.

Both components consist of stages that include one stationary and one rotating element, but their purposes and arrangements differ. As illustrated in Figure 2.9, in a compressor, a rotor row is followed by a stationary vane row, while in a turbine, a stationary nozzle precedes a rotating rotor row. The stationary vanes in the compressor are responsible for further compressing the air trough diffuion processes, whereas the nozzles in the turbine decompress the airflow and guide it in the most efficient direction, maximizing the kinetic energy absorbed by the turbine blades.

A more detailed explanation of the compressor's operation is provided in the following sections.

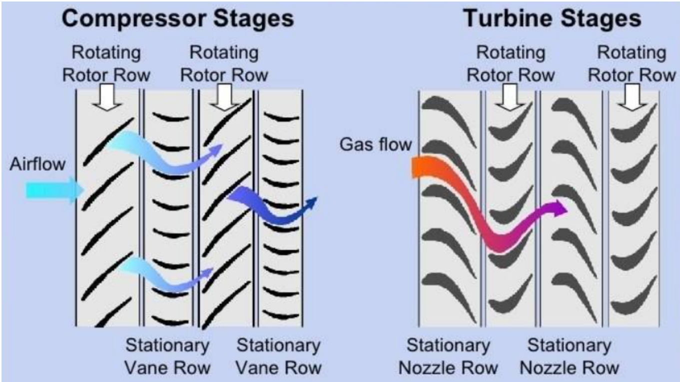

Figure 2.9: Axial Compressor vs Turbine flow [16]

2.2.3.4 Accessory Drive

As shown in Figure 2.10, the accessory drive delivers torque to the HPC to initiate engine start-up, as described in 2.2.1, enabling the compression process (red arrow path). During the engine's operating cycle, it supplies mechanical energy to both the aircraft and engine accessories (orange arrow path).

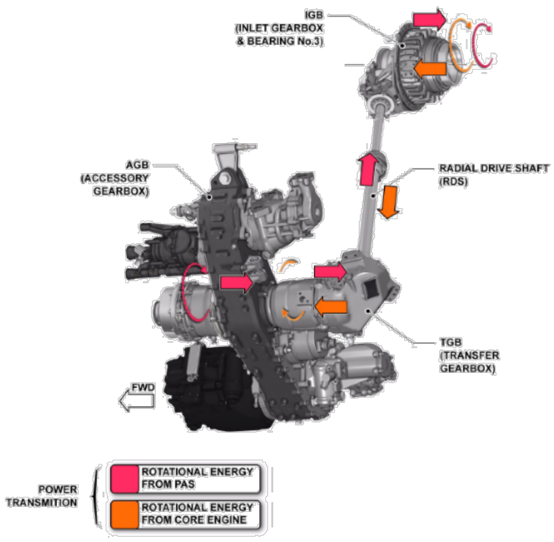

Figure 2.10: LEAP-1A Accessory Drives.[12]

3

Compressor

Being the purpose of this thesis *"Control and Optimization of High-Pressure Compressor Blade Dimensions and Clearances,"* it is crucial to study the operation of engine compressors, understanding their working principles and the key criteria that must be considered in order to improve the blades dimensions and clearences in engine reliability and performance.

This section highlights the key criteria, provides an overview of the module's operation, and explains how compressor wear during the engine's operating cycle affects its performance.

3.1 Axial Compressor

In gas turbine engines, there are two primary types of compressors: axial and centrifugal flow compressors. Both are driven by a shaft connected to the turbine; however, the axial type is easier to manufacture and can be designed to achieve higher pressure ratios. For this reason, commercial turbofan engines typically utilize this type of compressor, specifically in the LEAP-1A engine.

Higher pressure ratios are proven to improve fuel consumption as shown on Figure 3.1

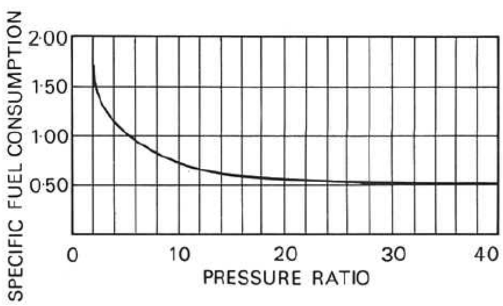

Figure 3.1: Specific Consumption.[7]

Using the LEAP-1A HPC as example, an axial compressor consists of one or more rotor assemblies which in turn can be one single part, representing a blisk, or a circumferential blade assembly. These assemblies are mounted between the 2 bearing in a casing which incorporate the stator vanes.

As mentioned in the previous sections, this compressor is a twin-spool, multi-stage unit consisting of 3+10 stages.

In other words, the compressor is composed of the LPC with three stages, followed by the HPC with ten stages. Additionally, the front fan can also be considered part of the compression system, as it contributes to air compression despite not being its primary function, effectively serving as the first stage of the LPC.

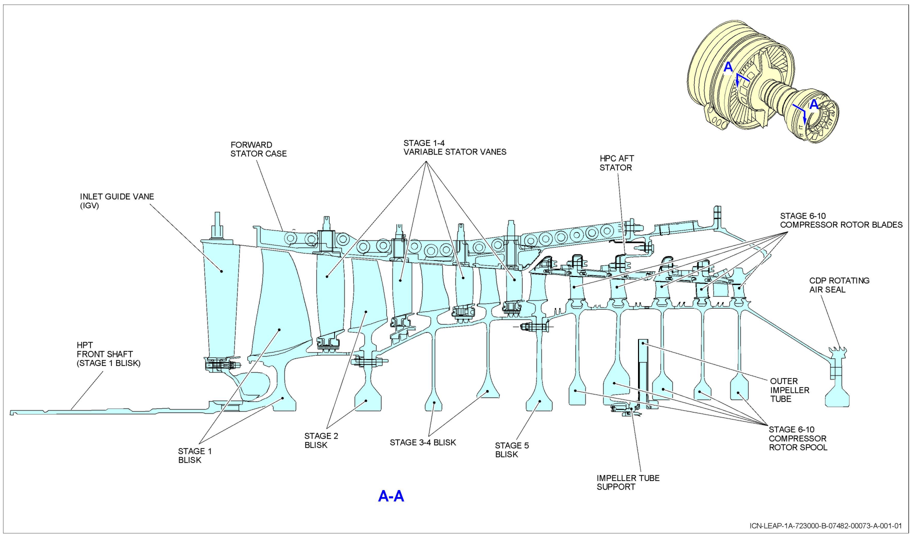

Figure 3.2: LEAP-1A HPC.[12]

With the engine running, the turbine transmits power to the compressor, driving it at high speed and ensuring a continuous airflow. As the air enters the LPC, it passes through the first rotor, where the rotating airfoil-shaped blades transfer kinetic energy to the airflow by increasing its tangential momentum. Simultaneously, pressure rises with the aid of the diffusion process. Next the air flows into the vanes where kinetic energy increase is converted in pressure increase by the same process found in the rotationary step.

The requirement for a high-pressure ratio on the shaft demands precise airflow control during engine operation to prevent airflow reversal, as a compressor inherently forces air from a low-pressure region to a higher-pressure zone. To achieve this, the guide vanes in the initial four stages functions as Variable Stator Vanes (VSV's), followed by fixed stator vanes in the subsequent stages. These variable vanes progressively close at lower airflow speeds to maintain an optimal air angle on the downstream rotor blades, preventing reverse flow and avoiding compressor stall.

During each stage the increase of pressure is relatevely small as shown in Figure 3.3 in order to avoid air breakaway at the blades and subsequent blade stall. On another hand, the multi-stage process alows the LEAP to achieve an Overall Pressure ratio of 40:1. This ratio represents the Pressure ratio of all the engine not just the compressor.

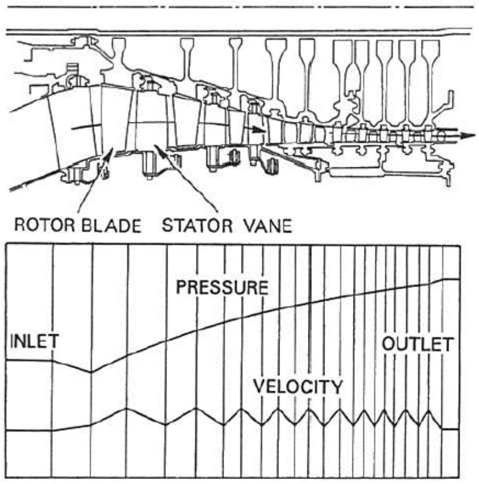

Figure 3.3: Axial Compressor Diagram and Pressure/Velocity Distribution.[7]

3.2 Blisks vs Bladed disks

In Figure 3.4, the HPC of the LEAP-1A engine is shown, consisting of five blisks, an impeller tube support, a five-stage rotor, and a rotating seal.

The incorporation of blisks in compressors represents a significant innovation in the LEAP-1A design compared to previous-generation turbofan engines. This advancement was introduced in aviation to enhance engine performance. Blisks significantly reduce rotor weight compared to conventional aero-engine disks. Since compressor and turbine disks contribute to over 20% of the engine's structural weight, their design presents numerous static and dynamic challenges.

From a design perspective, traditional bladed disks require the assembly of multiple components with different connection features, such as airfoil roots, disk roots, and locking mechanisms. In contrast, a blisk integrates all these elements into a single part, leading to several benefits:

- A reduction in the total number of parts, contributing to lower overall weight and faster assembly.
- Fewer contact surfaces, minimizing gaps where airflow could infiltrate and disrupt engine operation.
- Eliminates dovetails and its associated issues such as its wheight and propensity for leakeges.
- Simplified assembly during both production and maintenance, resulting in lower manufacturing costs and shorter lead times.

- The use of blisks implie bigger clearence between the blade tip and the stator which impacts engines performance.

However, blisks present significant drawbacks when compared to bladed disks, particularly in terms of maintenance and repairability. In the event of damage to an individual airfoil, the entire blisk must be replaced, leading to considerably higher costs than replacing a single blade. Additionally, as a single integrated component, the blisk eliminates the option of using different materials for the airfoil and the disk. The increased rigidity of the blisk also results in a lack of damping, which reduces its fatigue resistance.

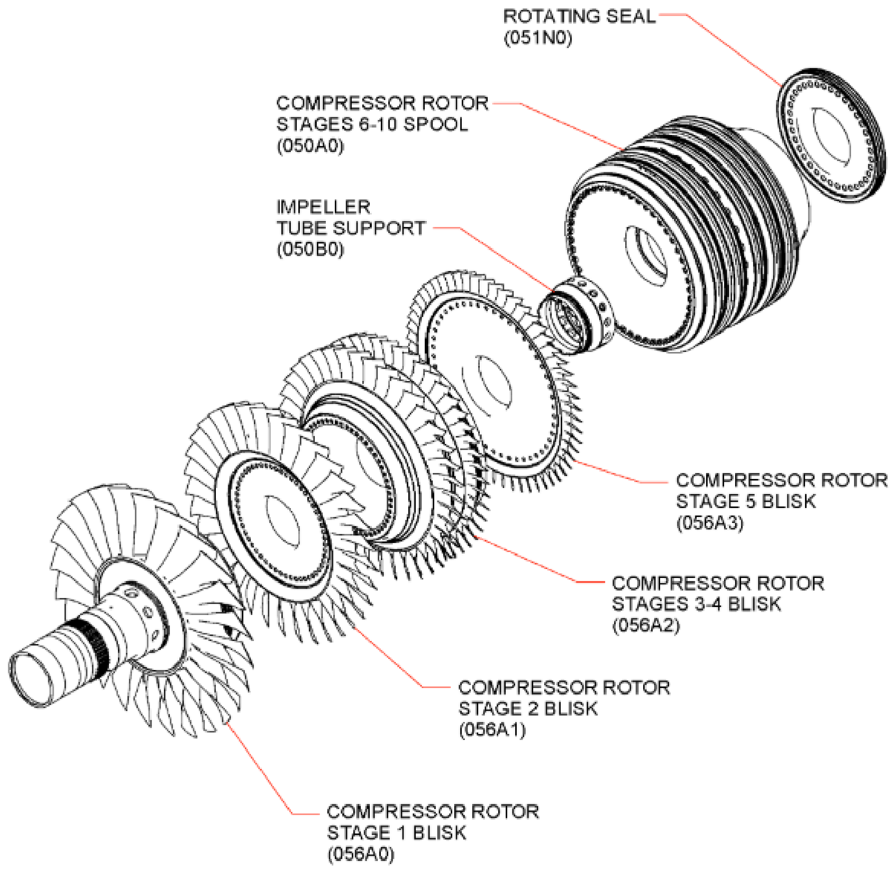

Figure 3.4: LEAP-1A HPC. [12]

3.3 Rotor Blades

As previously described, the HPC of the LEAP-1A consists of 10 stages, with the first five rotors designed as blisks and the last five as disks with fixed rotor blades. The attachment of these blades to the disk can be achieved through two different methods: axial or circumferential fixing, as illustrated in Figure 3.5.

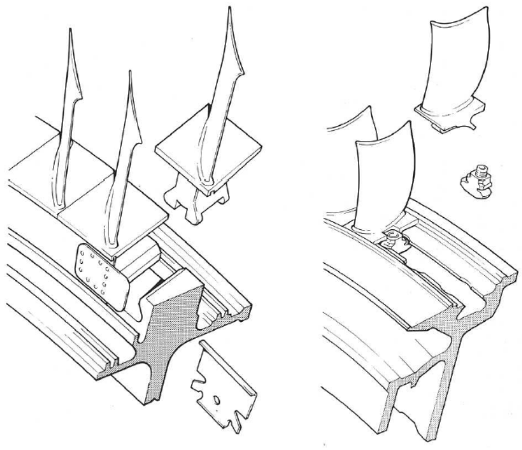

Figure 3.5: Axial Fixing on the left and circumferential on the right.[7]

The blades and disk shown in Figure 3.5 are not actual LEAP-1A components but merely illustrative examples.

The blades of the last five stages of the HPC are made from Inconel 718 and Inconel 718Plus. Inconel 718 is used in the first two stages, while Inconel 718Plus is used in stages 8, 9, and 10.

This material differs from the the blades found on the LPC or the blisks since with the increase of pressure temperature also rises.

INCONEL alloy 718 (UNS N07718/W.Nr. 2.4668) is a high-strength, corrosion-resistant nickel chromium material used at -252.78 to 704.44°C. [10]

Focusing on the last five stages of the HPC, in alignment with the objectives of this thesis, it is crucial to understand which dimensions impact the engine's performance, particularly as blade dimensions undergo changes due to excessive wear and usage, ultimately affecting engine performance and reliability.

TAP ME technicians are responsible for monitoring the most critical dimensions during the engine repair process.

These dimensions are specified in [12] and are illustrated in Figure 3.6. Based on this, the critical dimensions can be defined as follows: tip chord length (CH), blade tip length (H), leading edge thickness (TL), and trailing edge thickness (TU).

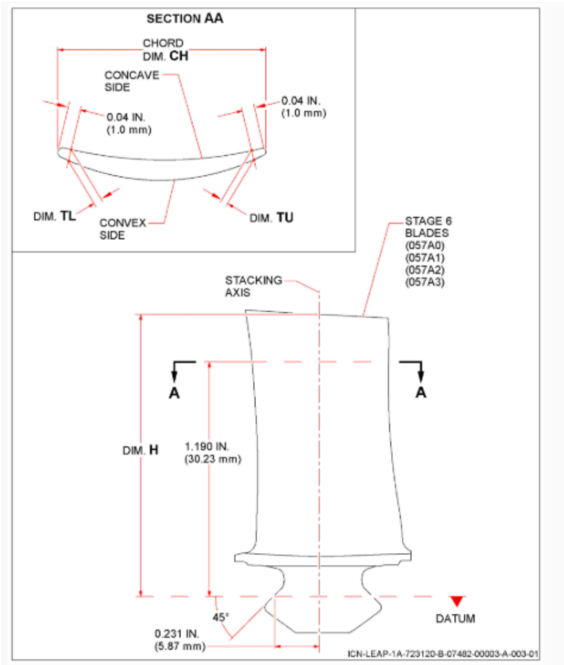

Figure 3.6: Stage 6 Blade Dimension Check.[12]

In each stage of the HPC, the blades can be categorized into three types: narrow body blades, wide body blades, and locking blades. The narrow and wide body blades are used to adjust the platform gaps, ensuring proper assembly and optimal aerodynamic performance. The locking blades, on the other hand, incorporate locking mechanisms that secure them in place, preventing movement during engine operation. The correct selection and placement of these blade types are essential to maintaining structural integrity and performance within the compressor. Therefore, ensuring the correct gap between the blades during the repair process is crucial to maintaining proper assembly, aerodynamic efficiency, and overall engine reliability.

3.4 Degradation Mechanisms of Compressor Blades

The degradation of compressor blades is a critical factor affecting engine performance and reliability. Commercial aircraft engines operate in diverse environments, exposing the engine core to various particles and contaminants.

These ingested particles, collectively known as Foreign Object Damage (FOD), include sand, metal fragments, birds, and other debris. The ingestion of such contaminants has two main consequences: if the particle is a hardbody, it can cause direct erosion and structural damage to the blades, leading to dimensional loss. In contrast, if the particle is a softbody, such as a bird, it can obstruct airflow, causing performance degradation or even severe engine failure.

In particular, this section examines the impacts of FOD on the geometry of compressor blades. The ingestion of particles during the engine cycle can lead to a reduction in blade chord, loss of blade thickness, alteration of the leading and trailing edge shapes, thinning of the blade trailing edge, blunting of the leading edge, and an increase in surface roughness.

Alterations in the blade geometry, such as changes in chord length, thickness loss, and alterations to the leading and trailing edges, result in increased clearance losses at the blade tips, higher frictional losses, and a significant reduction in off-idle and open beta stall margins. In Figure 3.7 its possible to observe the damages caused on the leading edge by continuous erosion. [15]

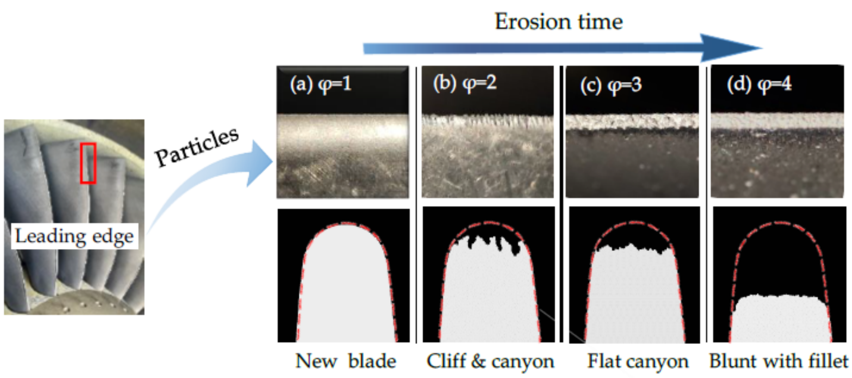

Figure 3.7: The effect on erosion trough time on the leading edge of a compressor blade [15]

These effects influence HPC efficiency and, consequently, engine performance. In particular, compressor blade erosion, coupled with efficiency losses throughout the engine, can increase fuel consumption by nearly 1 percent compared to new blades (see Figure 3.8) [15].

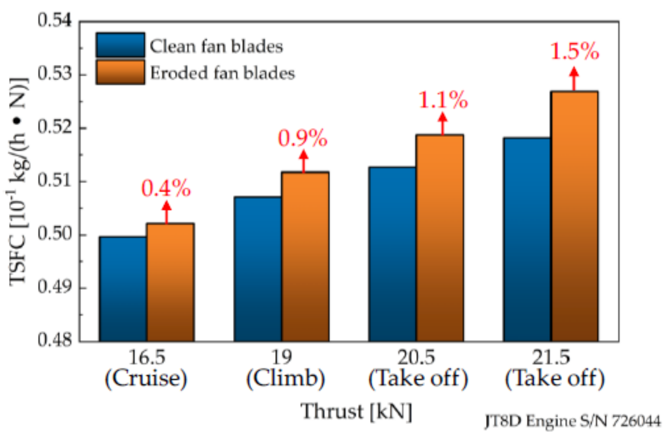

Figure 3.8: Comparison of thrust-specific fuel consumption (TSFC) between eroded and new compressor blades.[15]

4

Dimensional Inspection and Measurement Equipment

This chapter introduces the equipment and methodology that can be used for dimensional inspection in engine component analysis. Keeping parts within the required tolerances is essential for ensuring performance and durability. A 3D scanner makes it possible to generate a digital model of the components, while a coordinate measuring machine (CMM) allows for precise measurement and comparison with nominal dimensions. These tools help improve the accuracy of the analysis and support potential optimization of the components at TAP ME Engine Shop.

The Engine Shop at TAP ME has a specialized Dimensional Inspection department responsible for verifying component dimensions in accordance with the manual, ensuring optimal engine performance and reliability.

4.1 Available Measurement Equipment

To ensure precise measurements, the department relies on advanced equipment, such as the Creaform HandySCAN 3D scanner, which captures highly accurate digital models of components, and the Mitutoyo Euro-C 121210 coordinate measuring machine (CMM), which provides detailed dimensional and geometric analysis. By using these tools, the team can carry out thorough inspections, verify tolerances, and explore opportunities for improving component performance.

4.1.1 Creaform HandySCAN 3D scanner

The HandySCAN 3D is a high-precision laser scanner developed by Creaform, designed for portable 3D scanning of objects with complex geometries. It uses laser triangulation to capture detailed 3D models with high accuracy and resolution. It presents the following technical data:

- **Accuracy**: 0.025 mm (0.0009 in)

- **Volumetric Accuracy**: Up to 0.020 mm + 0.015 mm/m
- **Light Source**: 22–30 blue laser lines
- **Working Distance**: 200 to 750 mm
- **Recommended Part Size Range**: 0.05 – 4 m
- **Weight**: 0.94 kg

The HandySCAN 3D laser scanner is used in conjunction with VXelements, an integrated 3D software platform that allos real-time data acquisition, post-processing, and analysis.

During the development of this thesis, this equipment will enable the practice of reverse engineering. Using the HandySCAN 3D scanner, detailed physical data from the HPC blades can be captured, and with the VXelements software, the point cloud is transformed into a 3D Computer-Aided Design (CAD) model. This model can then be imported into SolidWorks for further analysis and used to design the workpiece, which will be employed in the CMM to securely hold the blades during measurement.

4.1.2 Mitutoyo Euro-C 121210

The CMM is a highly precise tool used to measure the geometry of parts and components. It works by using a probe that senses the physical contact with the object. While traditional CMMs rely on touch-trigger probes, there are other models that use laser or optical sensors to take measurements. The Mitutoyo Euro-C 121210 CMM is controlled by a computer and operates within a three-dimensional coordinate system.

This particular CMM is equipped with a Renishaw Revo-2, providing it with five degrees of freedom (DoF). In addition to moving along the three main axes, the machine can adjust the probe's angles, enabling it to measure even the most complex surfaces that would otherwise be difficult to reach. The machine setup includes a granite bed, probe, probe tree, arm, joystick, and specialized software, as shown in Figure 4.1.

Although four probes are available for use with the Renishaw Revo-2, only two are applicable to this project. Among them, the RSP2-3 is the sole probe that enables full five-degree-of-freedom operation. As illustrated in Figure 4.2, the first three DoFs (X, Y, and Z) are controlled by the CMM arm, while the remaining two (α, β) are executed by the probe itself.

Each probe has distinct characteristics suited for different tasks, as detailed in Table 4.1.

Table 4.1: Renishaw probes available at TAP

Probe	DoF	Scanning Capability	Sphere ∅
RSP2-3	5	2D	6mm
RSP3	3	3D	4mm

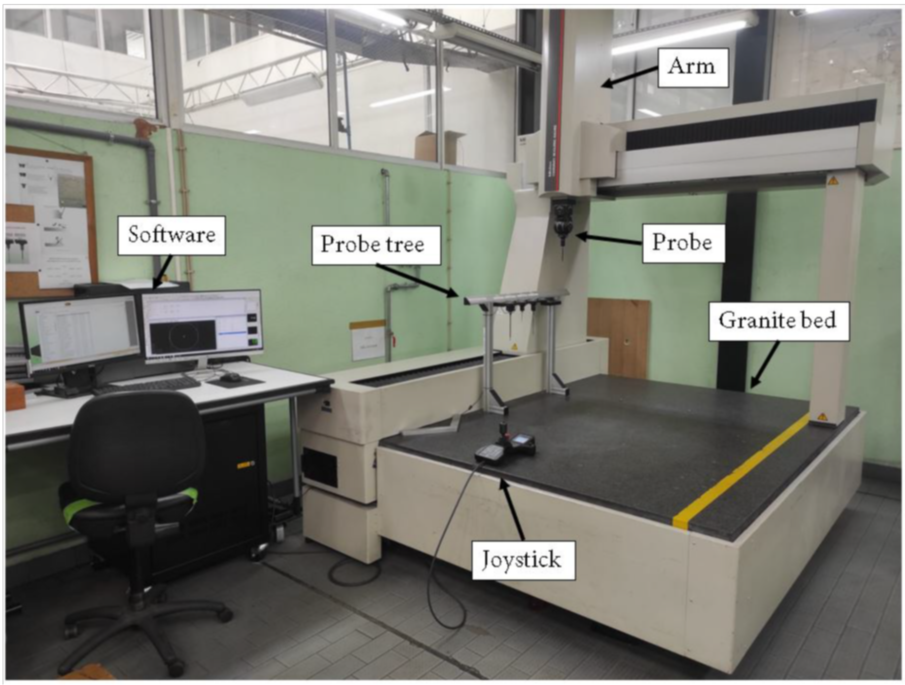

Figure 4.1: Mitutoyo Euro-C 121210 Components [15]

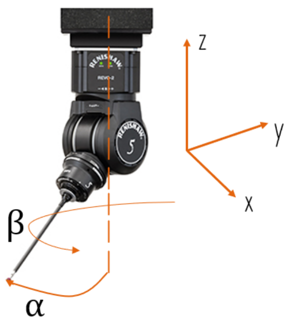

Figure 4.2: DOF of the Renishaw probe [14]

The integration of the CMM into this project plays a key role in ensuring that every high-pressure compressor rotor blade is measured quickly, accurately, and consistently. The development of a custom inspection program aims to enable the production team to measure entire sets of blades with minimal manual intervention, enhancing both efficiency and reliability.

Through the use of the CMM, it is possible to automatically verify critical dimensions, such as Chord Lenght (CL), Leading Edge Thickness (LET), Trailing Edge Thickness (TET), and overall airfoil geometry. This ensures that each blade meets the required tolerances while eliminating inconsistencies associated with manual measurement methods. Additionally, this automation reduces the workload of operators, allowing them to focus on other essential tasks while the machine performs the measurements.

Another significant advantage of the CMM is its ability to generate detailed inspection reports, facilitating the tracking of blade conditions over time. This capability extends beyond simple compliance verification, contributing to predictive maintenance strategies that enhance engine performance and reduce unexpected maintenance costs.

By incorporating this level of automation and precision into the inspection process, the proposed approach aims to streamline production, improve quality control, and establish a more efficient and standardized methodology for TAP's maintenance operations.

4.2 TAP ME: Previous Theses on Dimensional Inspection

In the past, several master's theses have been developed in collaboration with TAP ME, contributing to the improvement of measurement and inspection processes for aircraft engine components. One of these studies was conducted by Farinha, E. [5], focusing on the design of a fixture and the development of a measurement method for high-pressure compressor (HPC) rotor blades. This research continued the work initiated by Rendas, P. [13], who laid the foundation for the development of a fixture specifically designed for HPC rotor blade inspection.

Additionally, Baptista, F. [13] contributed to this field by developing a model that predicts the off-design performance of the CFM56-5B turbofan engine. More recently, Guerreiro, A. [8] worked on the development of a process to measure the exit flow area of the low-pressure turbine (LPT) nozzles from the same engine model. His study focused on creating an automated program for Coordinate Measuring Machine (CMM) inspection, addressing a previously undeveloped process within TAP ME's engine maintenance operations.

While previous studies have primarily focused on components of the CFM56-5B engine, this thesis aims to extend the dimensional inspection process to the HPC rotor blades of the LEAP-1A engine. One project involves developing an optimized CMM measurement program for assessing the blade chord to evaluate performance, utilizing data from the test bank. The second project focuses on measuring and controlling platform clearance to optimize the assembly process. These improvements, applied to both the LEAP and CFM engines, build on previous research, further advancing the continuous optimization of inspection methods to adapt to newer engine generations.

5 Problem Definition and Scope

This thesis tackles two key challenges in the assembly of HPC (High Pressure Compressor) blades. The goal is to ensure that the assembly process meets the required specifications and to better understand how blade geometry impacts engine performance.

The first challenge is to develop a process or tool that guarantees the correct assembly clearance for the blades. This clearance must comply with the specifications outlined in the engine manual, ensuring that the blades are assembled properly and function as intended.

The second objective is to create a reliable method for measuring the chord length of the blades and analyzing its correlation with engine performance in bench tests. By understanding this relationship, we can gain valuable insights into how small variations in manufacturing affect overall efficiency and explore ways to optimize the assembly process. Ultimately, this aims to guarantee and control engine performance according to operational needs.

Together, these objectives shape the scope of this work, which involves designing measurement tools, validating methodologies, and bridging the gap between manufacturing precision and engine performance.

In this chapter, the details of these challenges will be explored, along with the initial requirements and decisions that guided the approach taken. This will provide a comprehensive understanding of the context, constraints, and considerations that influenced the development of solutions throughout the project.

5.1 Blade Assembly Process and Clearance Requirements

This study focuses on the assembly of HPC stages 6 to 10, represented in Figure 5.1, as these are the stages that incorporate the blades under analysis, as previously mentioned. The assembly of HPC blades follows a standardized procedure to ensure precise positioning and compliance with the required specifications. The process begins with preparing the spool, where blade slots and wire seal grooves are cleaned and inspected. Contaminants are removed to ensure a smooth surface for blade insertion. Wire seals are then installed in the grooves, adhering to specified clearance tolerances to maintain structural integrity.

Figure 5.1: LEAP-1A HPC.

The blades are then inserted into the spool, following a controlled sequence to ensure a uniform distribution. During this step, each blade is checked for free movement within the dovetail slot, as any restrictions may indicate the need for replacement. After all blades are in place, locking blades are installed in designated positions to secure the assembly.

To finalize the assembly, locking lugs are positioned and their set screws are torqued to the required values. A detailed verification is performed to ensure that the locking lugs are correctly engaged within the spool's dovetail lock slot, preventing unintended movement. To confirm the correct platform clearance, the blades are shifted in one direction to determine the maximum gap, and measurements are taken to verify compliance with the permissible range. This clearance, referred to as Clearance R, is represented in Figure 5.2.If necessary, adjustments are made by replacing narrow-platform blades with wide-platform ones.

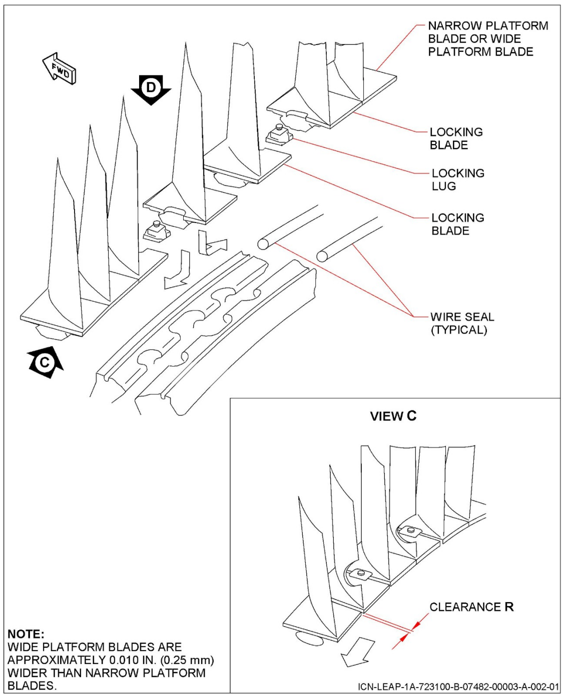

Figure 5.2: Stage Components and Clearence Representation

The measurement of the clearance is performed using a feeler gauge (with a corresponding image), ensuring precise determination of the gap. For each compressor stage, a predefined clearance value is specified, as presented in Table 5.1. In the aviation industry, these clearance values are typically provided in inches. However, throughout the development of this dissertation, all measurements have been converted to millimeters to maintain consistency.

Once the correct blade sequence and clearance are established, the assembly is reinstalled, and a final torque check is performed on the locking lugs. Ensuring that all components remain within the prescribed limits is critical to maintaining engine performance and durability, as deviations from the specified tolerances can lead to excessive wear, unwanted vibrations, or mechanical failures.

Stage	Assembly Clearance Tolerance [in]	Assembly Clearance Tolerance [mm]	Clearance [mm]
6	0.010-0.030	0.254-0.762	
7	0.010-0.030	0.254-0.762	
8	0.010-0.030	0.254-0.762	0.508
9	0.080-0.100	2.032-2.54	
10	0.149-0.169	3.7846-4.2926	

Table 5.1: Assembly clearance tolerances for different stages.

Currently, in TAP's ME Engine Shop assembly process, there is no method to anticipate this clearance before the assembly stage. As a result, if the measured clearance after assembly does not fall within the required specifications, additional wide-platform blades may need to be sourced from the supplier. This can introduce delays in the workflow, as the availability of the necessary blades depends on supplier lead times. As represented in Figure 5.2, wide-platform blades are approximately 0.25 mm wider than narrow blades, allowing for clearance adjustments when needed. Implementing a way to predict and control clearance earlier in the process would help streamline operations, reducing waiting times and improving overall efficiency.

As a first step, it is necessary to construct a nominal model of the blades from which further work can be carried out. This model will serve as the foundation for predicting and controlling assembly clearances, ensuring compliance with specifications, and improving process efficiency.

5.1.1 Defining Platform Tolerances and Tolerance Analysis Model for the Blade

One of the primary challenges in ensuring proper assembly clearance is the precision required to construct a nominal model of the blades. The assembly clearance depends on the individual blade dimensions, particularly the platform width, as these factor determine how the blades fit within the spool slots. To develop an effective process, it is essential to establish a nominal blade model with a precision level derived from the permissible clearance tolerances.

The required precision level can be derived from the assembly clearance by considering the maximum allowable variation that still maintains compliance. This ensures that the model reflects real-world manufacturing conditions and enables accurate clearance prediction.

To define the tolerance for the nominal model, a statistical approach is utilized, as described in [11]. Unlike the total interchangeability model, where tolerances are summed linearly, the statistical model considers the probability distribution of component variations. The assembly tolerance is calculated using the following equation:

$$T_{\text{conj}} = \sqrt{\sum_{i=1}^{n} t_i^2} \tag{5.1}$$

where:

- T_{conj} - Assembly Tolerance
- t_i - Part Tolerance

This approach reduces the overall tolerance accumulation, making it more suitable for large-scale production where component variations follow a normal distribution. By applying this model, it is possible to maintain a precise nominal blade model while accommodating natural manufacturing variations.

5.1.1.1 Calculation of Platform Dimensional Tolerance for Each Blade Type and Stage Using the statistical model

To evaluate the dimensional tolerance for each compressor stage, the number of wide and narrow blades assembled in the engine was analyzed. Table 5.2 presents the distribution of wide and narrow blades for each stage, along with the total number of blades. The assembly data was collected from a motor assembled in the workshop to determine the exact number of blades used.

Stage	Wide Blades	Narrow Blades	Total Blades
6	26	36	62
7	24	33	57
8	24	39	63
9	23	37	60
10	26	38	64

Table 5.2: Number of wide and narrow blades per stage.

Using the equation 5.1, and considering an assembly tolerance of 0.508 mm, we analyze the case for stage 6, which has 26 wide blades and 36 narrow blades. Beign almost identical parts, its assumed that the wide body and narrow body blades present the same tolerance, $T_w = T_n$, the equation simplifies to:

$$T_{\text{conj}} = \sqrt{26T_w^2 + 36T_n^2} \tag{5.2}$$

$$T_{\text{conj}} = \sqrt{62T_w^2} = \sqrt{62}T_w \tag{5.3}$$

Since the total assembly tolerance is given as 0.508 mm:

$$0.508 = \sqrt{62}T_w \tag{5.4}$$

Solving for T_w:

$$T_w = \frac{0.508}{\sqrt{62}} = 0.0646 \text{ mm} \tag{5.5}$$

Thus, the tolerance for each blade in stage 6 is approximately **0.0646 mm**.

Based on this analysis, the clearance values were calculated. Table 5.1.1.1 presents the obtained results.

These calculations, derived from workshop data and statistical analysis, ensure that the clearance assessment aligns with real assembly conditions. Furthermore, they provide insight into the required precision needed to develop a nominal model that enables a feasible and applicable solution.

Stage	Clearance (mm)	Tw = Tn
6		0,0645
7		0,0673
8	0.508	0.0640
9		0,0656
10		0,0635

Table 5.3: Computed clearance values per stage.

5.1.1.2 Calculation of Platform Dimensional Tolerance for Each Blade Type and Stage Using the Total Interchangeability Model

To assess the dimensional tolerance for each compressor stage under the total interchangeability model, we assume that all blades—wide and narrow—must individually conform to the overall assembly tolerance. This approach does not take into account statistical variations and instead assumes that each blade directly contributes to the total variation without reduction factors. The total interchangeability model represents a worst-case scenario and serves as a reference to highlight its impracticality compared to statistical models.

Using the same distribution of wide and narrow blades from Table 5.2, we analyze the tolerance requirement for each stage. The total tolerance allocation assumes that each blade's tolerance adds directly to the overall variation, leading to a simplified summation approach:

$$T_{\text{conj}} = (26+36)T_w = 62T_w \tag{5.6}$$

Given that the total assembly tolerance remains at 0.508 mm:

$$0.508 = 62T_w \tag{5.7}$$

Solving for :

$$T_w = \frac{0.508}{62} = 0.00819 \text{ mm} \tag{5.8}$$

Thus, under the total interchangeability model, each blade in stage 6 would require an individual tolerance of approximately 0.00819 mm, which is significantly tighter than the 0.0646 mm derived from the statistical model.

Applying the same method to other stages yields the results presented in Table 5.4.

These results clearly indicate that the total interchangeability model imposes unrealistically strict tolerances on each blade, making it practically infeasible for manufacturing and assembly. This reinforces the necessity of using statistical models to optimize tolerance allocation while maintaining feasible manufacturing constraints.

Stage	Clearance (mm)	(Total Interchangeability)
6	0.508	0.00819
7	0.508	0.00891
8	0.508	0.00806
9	0.508	0.00847
10	0.508	0.00782

Table 5.4: Computed clearance values per stage using total interchangeability.

As such, in this work, the statistical model was chosen as the reference for tolerance calculations, as it provides a more realistic and achievable approach while ensuring the necessary precision for assembly.

5.1.2 Analysis of Measurement Equipment Accuracy for Geometric Validation

Following this analysis, the next steps involve evaluating the available equipment previously mentioned in 4, specifically the Creaform HandySCAN 3D scanner and the Mitutoyo Euro-C 121210 CMM. While the application of reverse engineering using the scanner enables the creation of a model, its lower accuracy on edges may compromise the precision required to resolve the problem. Therefore, it is necessary to use the CMM to obtain the geometry with the required accuracy. Additionally, the scanner enables the development of the CMM fixture, which will be designed using knowledge from previous dissertations.

The accuracy of the available equipment is as follows:

- HandyScan accuracy: 0.001 in (0.0254 mm)
- Peripheral tape accuracy: 0.0005 in (0.0127 mm)
- CMM accuracy: 0.00001 in (0.00000254 mm)

These values highlight the significant difference in measurement precision, reinforcing the need for a combined approach to achieve the required accuracy.

It is essential to follow the golden rule of metrology, known as George Berndt's law, which states that "the measurement uncertainty should not exceed 1/10 of the tolerance of the dimension being controlled." This principle ensures that the selected measurement tools provide results with a level of precision suitable for the given tolerances.

It is important to note that the CMM at TAP is currently inoperative (INOP), and during this project, TAP proceeded with the purchase of a new machine. However, to expedite the work, a machine was made available by the R&D department of Hanon Systems, which will allow progress in the project and facilitate the measurement of the platform profile of the blades to properly define the dimensions required for the work

Therefore, while the HandyScan may be useful for generating general models, the CMM will be the preferred equipment to ensure that the calculated tolerances, particularly values as small as 0.0646 mm (for stage 6), are met with precision. The combination of these tools will provide a robust and accurate approach to validating and controlling assembly tolerances, ensuring that the blades fit correctly and optimizing engine performance.

5.1.3 Spool Measurements and Specifications

To ensure precise assembly and proper clearance for the HPC blades, it is essential to define the key dimensions of the spool. The spool serves as the foundational structure for blade installation, and its dimensions directly impact the assembly process.

These dimensions play a crucial role in determining the fit and function of the HPC blades. The slot width and depth directly influence how securely the blades are held in place, while the groove width and depth are vital for the proper installation of wire seals. Additionally, platform clearance values dictate the permissible gap between adjacent blades, ensuring compliance with operational specifications.

The diameter measurements were obtained using a Peripheral tape on a previously used spool available on TAP's engine shop. During the measuring process it was possible to differenciate two diferent spool diameteres per stage,$\varnothing Up$ and $\varnothing Down$, represented in Figure 5.3. Having this two different diameters per stage implies that the blades do not rest on the spool over two equal diameters, resulting in a lack of symmetry between these two geometries. Table 5.5 presents the measured diameters. Later on section **??** this subject is studied in more depth.

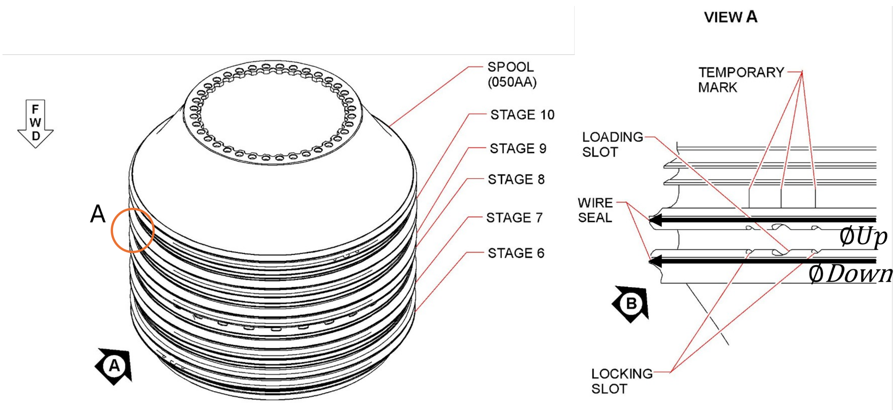

Figure 5.3: Stage Components and Clearence Representation

By integrating these spool measurements into the assembly process analysis, it is possible to predict and optimize the blade fitting conditions before final assembly, reducing rework and improving overall efficiency.

Stage	ØUp [in]	ØDown [in]	ØUp [mm]	ØDown [mm]
10	15.675	15.69	398.145	398.526
9	15.704	15.66	398.882	397.764
8	15.670	15.62	398.018	396.748
7	15.620	15.69	396.748	398.526
6	15.545	15.52	394.843	394.208

Table 5.5: Diameter values for each stage

5.1.4 Contact Point Analysis Between Blades

This section aims to identify the exact regions where contact occurs between adjacent blade platforms. The 3D scans of the blades do not offer sufficient resolution to precisely capture the geometry and curvature of the contact surfaces. Therefore, a more detailed analysis is required in these specific areas to understand how the platforms interact and to accurately determine where contact takes place during assembly and operation. To better understand how these surfaces interact, a two-part analysis was carried out: first through visual inspection of used blades to identify real contact marks, and then through precise CMM measurements to characterise the geometry of the contact areas.

To improve the dimensional characterization of the contact area between adjacent blade platforms, two reference profiles were defined: the left profile and the right profile. This naming helps simplify and organize the analysis that follows, making it easier to distinguish the different contact zones being assessed. Figure 5.4 shows the selected profiles and their location on the blade geometry.

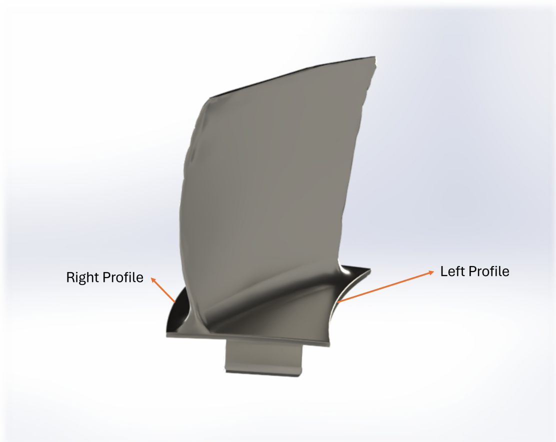

Figure 5.4: Contact zones identified by surface wear.

5.1.4.1 Visual Inspection of Used Blades: Identifying Contact Zones

Initially, to understand where contact between adjacent blades occurs, five used narrow-body blades and five used wide-body blades were randomly selected from a worn LEAP-1A engine. Since these blades had already been in operation, the wear marks left by contact made it possible to visually identify the contact zones. Evidence of contact was observed mainly at the extremities of both profiles, as shown in Figure 5.5.

Figure 5.5: Contact zones identified by surface wear.

As shown in Figure 5.6, this contact pattern consistently appears across all the selected blades, confirming the repeatability of the phenomenon.

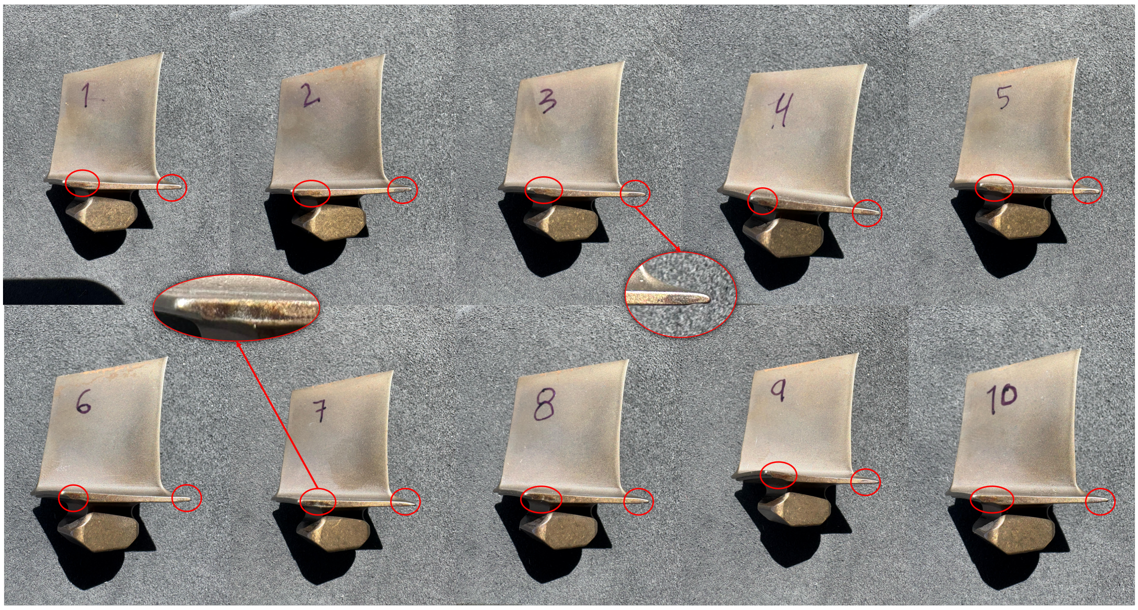

Figure 5.6: Contact zones identified by surface wear.

The presence of consistent wear marks at the extremities of both profiles suggests that these are the actual contact points during blade assembly. This indicates that the platform clearance is effectively defined at these specific regions, making them the critical areas to consider when trying to understand how the assembly gap is established in practice.

5.1.4.2 Dimensional Characterization of Blade Contact Surfaces Using CMM

As established in Section 5.1.1, the dimensional tolerances required for blade manufacturing are extremely tight. For example, using the statistical tolerance model, the sixth stage of the HPC assembly demands a manufacturing tolerance of just **0.0645 mm** per blade. According to the metrology rule referred in 5.1.2, the measurement uncertainty must be no greater than one-tenth of the tolerance. Therefore the required measurement uncertainty must be below **0.00645 mm (6.45 μm)**.

As previously discussed, the HandySCAN 3D scanner, although highly useful for general reverse engineering tasks, does not provide the necessary accuracy in critical areas such as blade edges or contact surfaces. Its resolution is insufficient to guarantee the precision needed for meaningful dimensional comparison at this scale.

For this reason, it became essential to resort to measurement by Coordinate Measuring Machine (CMM), which provides the required level of precision to properly define the problem dimensionally and allow for accurate blade analysis.

The CMM available at TAP ME normally offers a precision of 0.001 inches (25.4 μm). However, due to it being out of service at the time of this work, an alternative CMM was made available by the R&D department of Hanon Systems. This machine operates with a precision of **1.6 + L/350 μm**, where L is the length of the measured feature in millimetres.

For the measurements carried out on the contact profiles, this results in a measurement uncertainty of **1.6605 μm** for the left profile and **1.6614 μm** for the right profile—well within the required accuracy range for this analysis.

Before each measurement, the CMM performs an initial alignment process to establish the coordinate system (X, Y, and Z axes) and ensure that the fixation tool is correctly positioned. This procedure is illustrated in Figure 5.7, which shows the alignment sequence in three steps.

In the first step (left image), the probe detects four points on the base of the fixation tool to define the initial plane — the YX plane.

Next (middle and right images), the machine scans four points on each lateral side of the fixation tool, resulting in eight points in total. Based on these, it calculates an intermediate surface that defines the YZ plane.

Finally, a single point is probed on the front face of the fixation tool (right image), allowing the system to determine the XZ plane and complete the coordinate setup.

While this method ensures consistency in positioning, it also presents a limitation: the alignment is referenced to the fixation tool rather than the blade itself. As a result, slight geometric deviations between individual blades may go unnoticed, reducing the accuracy of contact surface comparisons.

In this analysis, the same ten randomly selected sixth stage blades previously examined for surface wear — five narrow-body and five wide-body — were measured to capture detailed geometric data from the contact zones and assess part-to-part variation.

The resulting coordinate system, defined through this alignment procedure, is represented in Figure 5.8, which was extracted from the CMM simulation software and visually illustrates the orientation of the X, Y, and Z axes relative to the fixture.

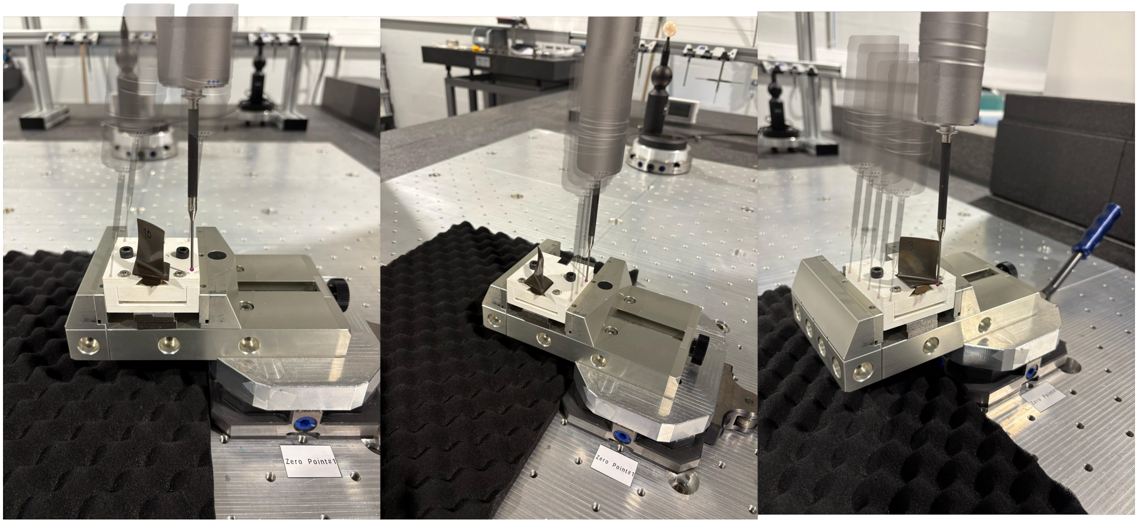

Figure 5.7: Contact zones identified by surface wear.

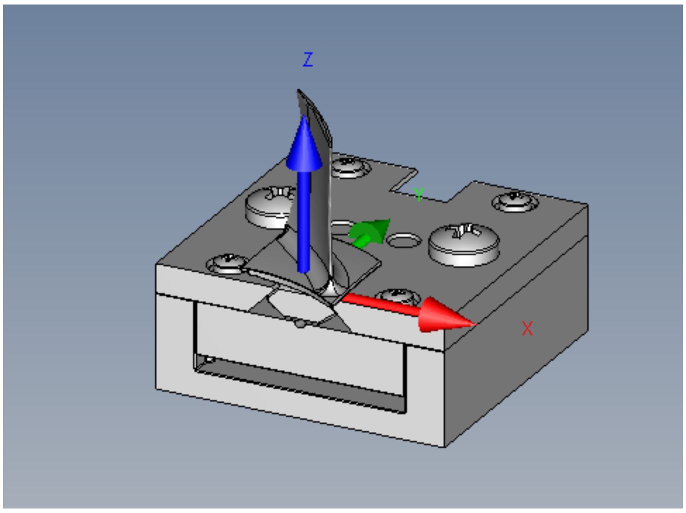

Figure 5.8: Contact zones identified by surface wear.

The CMM measurement procedure consisted of single passes along the contact profiles. For each blade, the probe performed three scan paths: one on the left profile and one on the right profile with 400 points each, and two additional passes on the left profile at different heights. These dense point clouds allowed for a detailed reconstruction of the contact surface geometry. Additionally, with the last two passes the system estimated the angle of the contact profile within the YZ plane to better understand the surface orientation. All individual measurements are presented in the annex, and the measured curvature radii are summarized in the following table.

Table 5.6: CMM measured radii at left and right profiles for Narrow and Wide Body blades.

Narrow Body Radius (mm)			Wide Body Radius (mm)		
Blade N°	**Left Profile**	**Right Profile**	**Blade N°**	**Left Profile**	**Right Profile**
1	30.7734	30.548	6	30.6168	30.6588
2	30.7584	30.545	7	30.5421	30.6623
3	30.7627	30.5403	8	30.5850	30.6342
4	30.7451	30.5411	9	30.5942	30.6323
5	30.7355	30.5327	10	30.6379	30.6614
	Avg 30.7550	**Avg** 30.5414		**Avg** 30.5952	**Avg** 30.6498

Table 5.7: Summary of average and variation between maximum and minimum CMM-measured radii.

	Narrow Body (mm)		Wide Body (mm)	
Profile	**Left**	**Right**	**Left**	**Right**
Average Radius	30.7550	30.5414	30.5952	30.6498
Max-Min Variation	0.0379	0.0153	0.0958	0.0300

Based on the results presented in Table 5.7, the average values of the measured radii for each profile were defined as the nominal dimensions to be used in the blade model. The corresponding variations between the maximum and minimum values measured for each profile are considered representative of the dimensional tolerance associated with each nominal value. This approach ensures that the nominal model reflects the actual manufacturing variability observed across the sampled blades.

Additionally, as shown in the reports presented in the appendix and previously referenced, these measurements also aimed to estimate the angle of the contact profile within the YZ plane. However, due to the complex geometry and the limited thickness available for probing, the resulting values showed significant variation between blades. This results are presented in Table 5.8

Table 5.8: Estimated angles of the contact profiles within the YZ plane (in degrees).

Left Profile Angle (°)	Right Profile Angle (°)
-23.0719	-34.9658
-31.6433	-34.7307
-36.5751	-36.2302
-35.0147	-37.0324
-38.9593	-32.0996

These results are presented in Table 5.8, which highlights the lack of consistency between the measured angles. Given this high variability, it was concluded that these values cannot be reliably used to define a nominal model for the contact profile geometry. Therefore, angle estimation was excluded from the subsequent dimensional analysis.

In the following chapters, if angle measurement becomes necessary, the measurement procedure will need to be revisited. This may involve using different probe paths or adopting a more suitable strategy to capture the angular orientation of these narrow surfaces with greater repeatability.

Bibliography

[1] K. Aainsqatsi. *Schematic Diagram of a 2-Spool, High-Bypass Turbofan Engine*. [Online; accessed 13-February-2025]. 2008-05. URL: https://commons.wikimedia.org/wiki/File:Turbofan_operation.png (cit. on p. 6).

[2] *Brochure LEAP fiches 2017*. Brochure document. 2017 (cit. on pp. 6, 7).

[3] A. Comercial. *Frota - TAP Air Portugal*. [Online; accessed 30-January-2025]. 2024-12. URL: https://www.aviacaocomercial.net/frotatap.htm (visited on 2024-12-01) (cit. on p. 3).

[4] M. A. Engines. *LEAP-1A/-1B Commercial Aircraft Engines*. [Online; accessed 13-February-2025]. 2025. URL: https://www.mtu.de/engines/commercial-aircraft-engines/narrowbody-and-regional-jets/leap-1a/-1b/ (cit. on p. 7).

[5] E. E. Farinha and M. J. A. Santos. *Fixture Design and CMM Program Development for Measuring of High Pressure Compressor Rotor Blades*. Co-adviser: Mário Almeida Santos. 2021 (cit. on pp. 1, 22).

[6] B. Fehrm. *Björn's Corner: New engine development. Part 22: High turbine technologies*. [Online; accessed 13-February-2025]. 2024-08. URL: https://leehamnews.com/2024/08/30/bjorns-corner-new-engine-development-part-22-high-turbine-technologies/ (cit. on p. 8).

[7] R. R. A. Group. *The Jet Engine*. Fifth. Rolls-Royce plc, 2007. ISBN: 0902121235 (cit. on pp. 4, 5, 12, 14, 16).

[8] A. C. D. S. Guerreiro. *Development of a Process to Measure the Exit Flow Area of the Low Pressure Turbine Nozzle from the CFM56-5B Engine*. Thesis or internal report. N/A (cit. on p. 22).

[9] J. M. Lourenço. *The NOVAthesis LaTeX Template User's Manual*. NOVA University Lisbon. 2021. URL: https://github.com/joaomlourenco/novathesis/raw/master/template.pdf (cit. on p. ii).

[10] S. Metals. *INCONEL 718 Alloy*. [Online; accessed 06-February-2025]. URL: https://www.specialmetals.com/documents/technical-bulletins/inconel/inconel-alloy-718.pdf (visited on 2025-02-06) (cit. on p. 16).

[11] A. Mourão. *UNIVERSIDADE NOVA DE LISBOA FACULDADE DE CIÊNCIAS E TECNOLOGIA DEPARTAMENTO DE ENGENHARIA MECÂNICA E INDUSTRIAL MESTRADO INTEGRADO EM ENGENHARIA MECÂNICA DIMENSIONAMENTO FUNCIONAL E TECNOLÓGICO*. 2004 (cit. on p. 26).

[12] T. A. Portugal. *Manual de Manutenção Oficinal LEAP1A - Hardware*. 2020 (cit. on pp. 8–11, 13, 15–17).

[13] P. Rendas. *Fixture Design and Process Development for High Pressure Compressor Rotor Blades Measuring in Aircraft Engine Maintenance*. 2021, pp. 1–45 (cit. on p. 22).

[14] Renishaw. *Renishaw: Enhancing Efficiency in Manufacturing and Healthcare*. https://www.renishaw.com/en/renishaw-enhancing-efficiency-in-manufacturing-and-healthcare--1030. Accessed: 2025-02-13. 2025 (cit. on p. 21).

[15] L. Shi et al. "A Review on Leading-Edge Erosion Morphology and Performance Degradation of Aero-Engine Fan and Compressor Blades". In: *Energies* 16 (7 2023-04), p. 3068. ISSN: 1996-1073. DOI: 10.3390/en16073068 (cit. on pp. 18, 21).

[16] Trent1. *Axial Compressor and Turbine Operation*. https://www.phase-trans.msm.cam.ac.uk/mphil/Trent1/sld011.htm. Accessed: 2025-02-13. n.d. (Cit. on p. 11).

A

Appendix

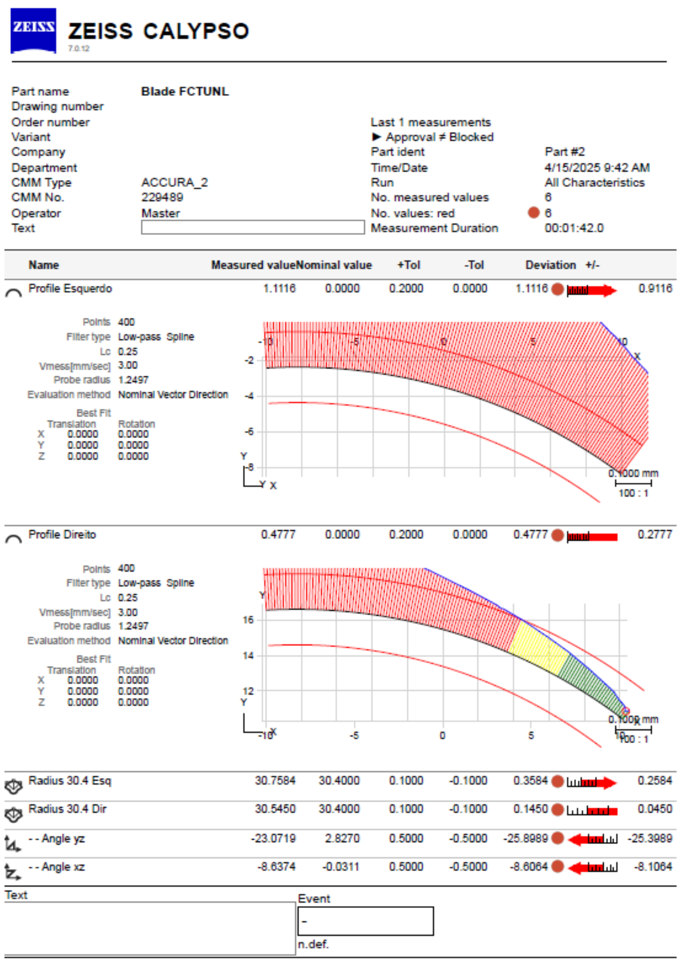
ZEISS CALYPSO
7.0.12

Part name Blade FCTUNL
Drawing number
Order number
Variant
Company
Department
CMM Type ACCURA_2
CMM No. 229489
Operator Master
Text

Last 1 measurements
► Approval ≠ Blocked
Part ident Part #2
Time/Date 4/15/2025 9:42 AM
Run All Characteristics
No. measured values 6
No. values: red 6
Measurement Duration 00:01:42.0

Name	Measured value	Nominal value	+Tol	-Tol	Deviation	+/-
Profile Esquerdo	1.1116	0.0000	0.2000	0.0000	1.1116	0.9116
Profile Direito	0.4777	0.0000	0.2000	0.0000	0.4777	0.2777
Radius 30.4 Esq	30.7584	30.4000	0.1000	-0.1000	0.3584	0.2584
Radius 30.4 Dir	30.5450	30.4000	0.1000	-0.1000	0.1450	0.0450
- - Angle yz	-23.0719	2.8270	0.5000	-0.5000	-25.8989	-25.3989
- - Angle xz	-8.6374	-0.0311	0.5000	-0.5000	-8.6064	-8.1064

Profile Esquerdo and Profile Direito (each):
Points 400
Filter type Low-pass Spline
Lc 0.25
Vmess[mm/sec] 3.00
Probe radius 1.2497
Evaluation method Nominal Vector Direction
Best Fit
Translation Rotation
X 0.0000 0.0000
Y 0.0000 0.0000
Z 0.0000 0.0000

Text
Event
-
n.def.

Figure A.1: Profile Measurement Report Blade 1

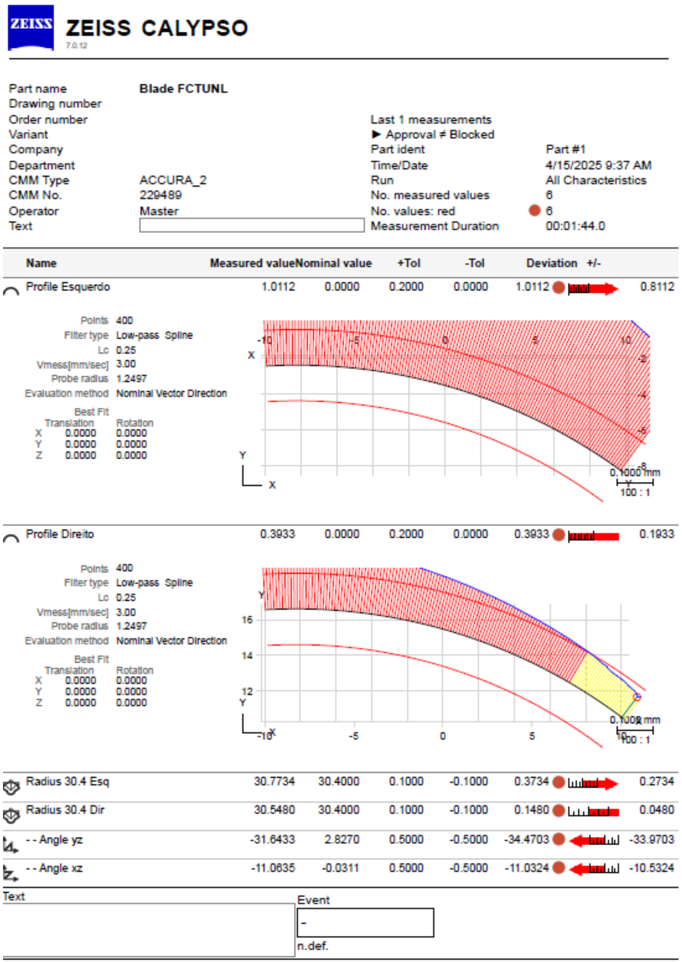

ZEISS CALYPSO

Part name	Blade FCTUNL		
Drawing number			
Order number		Last 1 measurements	
Variant		► Approval ≠ Blocked	
Company		Part ident	Part #1
Department		Time/Date	4/15/2025 9:37 AM
CMM Type	ACCURA_2	Run	All Characteristics
CMM No.	229489	No. measured values	6
Operator	Master	No. values: red	6
Text		Measurement Duration	00:01:44.0

Name	Measured value	Nominal value	+Tol	-Tol	Deviation	+/-
Profile Esquerdo	1.0112	0.0000	0.2000	0.0000	1.0112	0.8112
Profile Direito	0.3933	0.0000	0.2000	0.0000	0.3933	0.1933
Radius 30.4 Esq	30.7734	30.4000	0.1000	-0.1000	0.3734	0.2734
Radius 30.4 Dir	30.5480	30.4000	0.1000	-0.1000	0.1480	0.0480
- - Angle yz	-31.6433	2.8270	0.5000	-0.5000	-34.4703	-33.9703
- - Angle xz	-11.0635	-0.0311	0.5000	-0.5000	-11.0324	-10.5324

Profile Esquerdo / Profile Direito:
Points 400
Filter type Low-pass Spline
Lc 0.25
Vmess[mm/sec] 3.00
Probe radius 1.2497
Evaluation method Nominal Vector Direction
Best Fit
Translation X 0.0000 Y 0.0000 Z 0.0000
Rotation 0.0000 0.0000 0.0000

Text
Event
-
n.def.

Figure A.2: Profile Measurement Report Blade 2

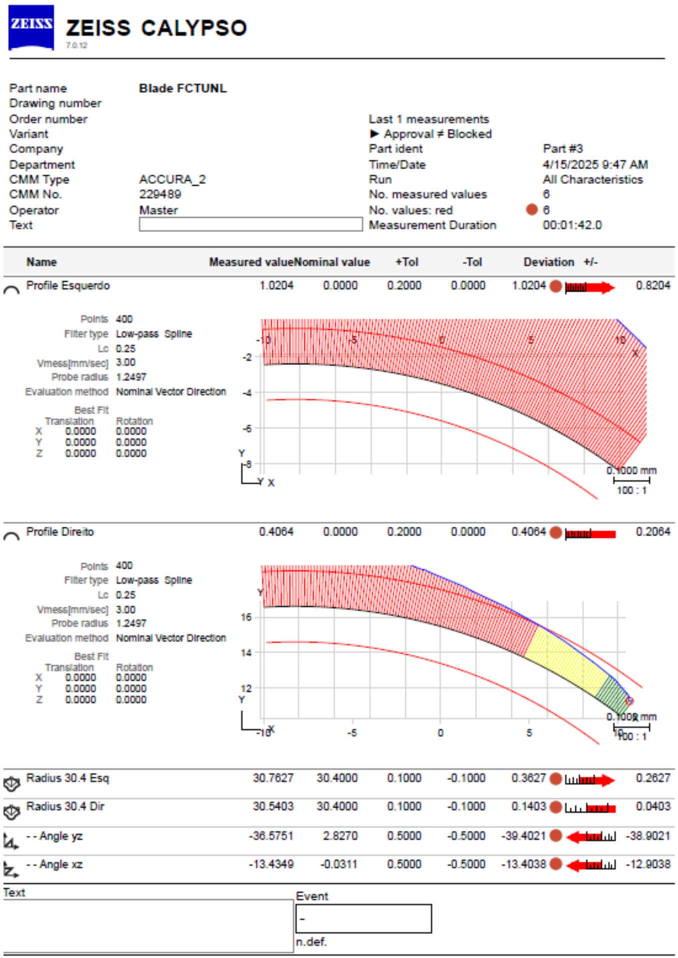

ZEISS CALYPSO
7.0.12

Part name	Blade FCTUNL		
Drawing number			
Order number		Last 1 measurements	
Variant		▶ Approval ≠ Blocked	
Company		Part ident	Part #3
Department		Time/Date	4/15/2025 9:47 AM
CMM Type	ACCURA_2	Run	All Characteristics
CMM No.	229489	No. measured values	6
Operator	Master	No. values: red	6
Text		Measurement Duration	00:01:42.0

Name	Measured value	Nominal value	+Tol	-Tol	Deviation	+/-
Profile Esquerdo	1.0204	0.0000	0.2000	0.0000	1.0204	0.8204
Profile Direito	0.4064	0.0000	0.2000	0.0000	0.4064	0.2064
Radius 30.4 Esq	30.7627	30.4000	0.1000	-0.1000	0.3627	0.2627
Radius 30.4 Dir	30.5403	30.4000	0.1000	-0.1000	0.1403	0.0403
- - Angle yz	-36.5751	2.8270	0.5000	-0.5000	-39.4021	-38.9021
- - Angle xz	-13.4349	-0.0311	0.5000	-0.5000	-13.4038	-12.9038

Profile Esquerdo / Profile Direito:

Points	400
Filter type	Low-pass Spline
Lc	0.25
Vmess[mm/sec]	3.00
Probe radius	1.2497
Evaluation method	Nominal Vector Direction

Best Fit	Translation	Rotation
X	0.0000	0.0000
Y	0.0000	0.0000
Z	0.0000	0.0000

Text
Event
-
n.def.

Figure A.3: Profile Measurement Report Blade 3

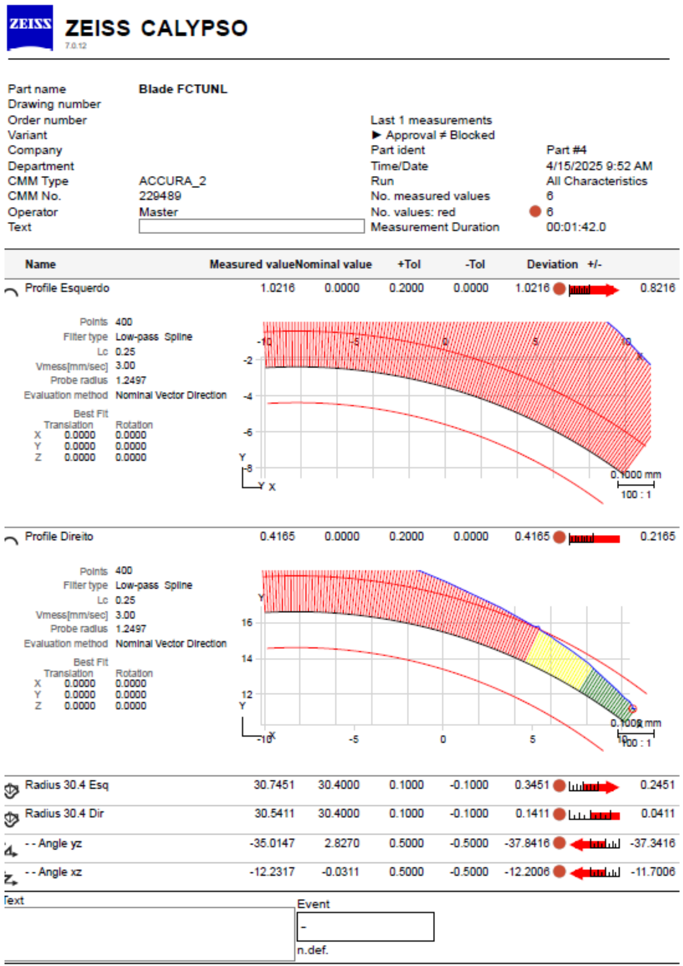

ZEISS CALYPSO

Part name	Blade FCTUNL		
Drawing number			
Order number		Last 1 measurements	
Variant		► Approval ≠ Blocked	
Company		Part ident	Part #4
Department		Time/Date	4/15/2025 9:52 AM
CMM Type	ACCURA_2	Run	All Characteristics
CMM No.	229489	No. measured values	6
Operator	Master	No. values: red	6
Text		Measurement Duration	00:01:42.0

Name	Measured value	Nominal value	+Tol	-Tol	Deviation	+/-
Profile Esquerdo	1.0216	0.0000	0.2000	0.0000	1.0216	0.8216
Profile Direito	0.4165	0.0000	0.2000	0.0000	0.4165	0.2165
Radius 30.4 Esq	30.7451	30.4000	0.1000	-0.1000	0.3451	0.2451
Radius 30.4 Dir	30.5411	30.4000	0.1000	-0.1000	0.1411	0.0411
- - Angle yz	-35.0147	2.8270	0.5000	-0.5000	-37.8416	-37.3416
- - Angle xz	-12.2317	-0.0311	0.5000	-0.5000	-12.2006	-11.7006

Profile Esquerdo / Profile Direito:

Points	400
Filter type	Low-pass Spline
Lc	0.25
Vmess[mm/sec]	3.00
Probe radius	1.2497
Evaluation method	Nominal Vector Direction

Best Fit

	Translation	Rotation
X	0.0000	0.0000
Y	0.0000	0.0000
Z	0.0000	0.0000

Text

Event

n.def.

Figure A.4: Profile Measurement Report Blade 4

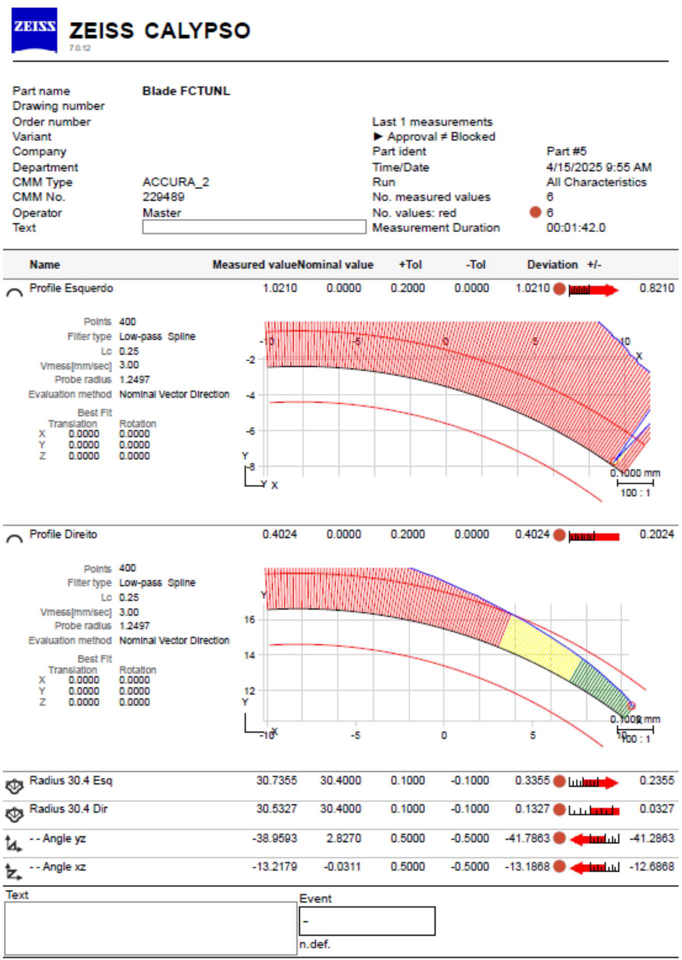
ZEISS CALYPSO
7.0.12

Part name	Blade FCTUNL		
Drawing number			
Order number		Last 1 measurements	
Variant		► Approval ≠ Blocked	
Company		Part ident	Part #5
Department		Time/Date	4/15/2025 9:55 AM
CMM Type	ACCURA_2	Run	All Characteristics
CMM No.	229489	No. measured values	6
Operator	Master	No. values: red	6
Text		Measurement Duration	00:01:42.0

Name	Measured value	Nominal value	+Tol	-Tol	Deviation	+/-
Profile Esquerdo	1.0210	0.0000	0.2000	0.0000	1.0210	0.8210
Profile Direito	0.4024	0.0000	0.2000	0.0000	0.4024	0.2024
Radius 30.4 Esq	30.7355	30.4000	0.1000	-0.1000	0.3355	0.2355
Radius 30.4 Dir	30.5327	30.4000	0.1000	-0.1000	0.1327	0.0327
- - Angle yz	-38.9593	2.8270	0.5000	-0.5000	-41.7863	-41.2863
- - Angle xz	-13.2179	-0.0311	0.5000	-0.5000	-13.1868	-12.6868

Profile Esquerdo / Profile Direito (each):
Points 400
Filter type Low-pass Spline
Lc 0.25
Vmess[mm/sec] 3.00
Probe radius 1.2497
Evaluation method Nominal Vector Direction
Best Fit

	Translation	Rotation
X	0.0000	0.0000
Y	0.0000	0.0000
Z	0.0000	0.0000

Text

Event
-
n.def.

Figure A.5: Profile Measurement Report Blade 5

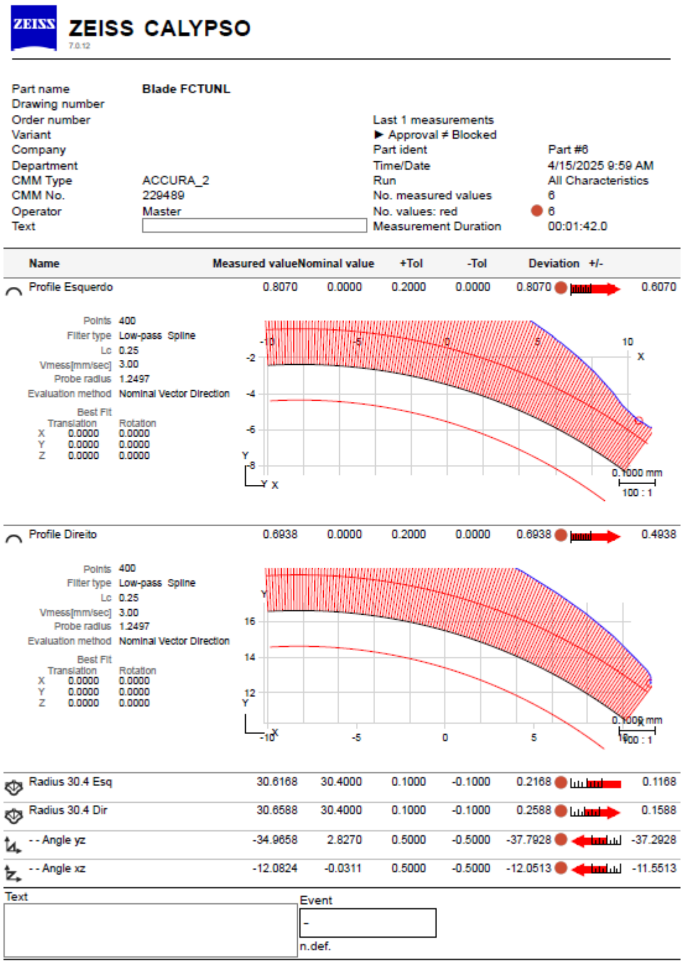
ZEISS CALYPSO
7.0.12

Part name	Blade FCTUNL		
Drawing number			
Order number		Last 1 measurements	
Variant		► Approval ≠ Blocked	
Company		Part ident	Part #6
Department		Time/Date	4/15/2025 9:59 AM
CMM Type	ACCURA_2	Run	All Characteristics
CMM No.	229489	No. measured values	6
Operator	Master	No. values: red	6
Text		Measurement Duration	00:01:42.0

Name	Measured value	Nominal value	+Tol	-Tol	Deviation	+/-
Profile Esquerdo	0.8070	0.0000	0.2000	0.0000	0.8070	0.6070
Profile Direito	0.6938	0.0000	0.2000	0.0000	0.6938	0.4938
Radius 30.4 Esq	30.6168	30.4000	0.1000	-0.1000	0.2168	0.1168
Radius 30.4 Dir	30.6588	30.4000	0.1000	-0.1000	0.2588	0.1588
- - Angle yz	-34.9658	2.8270	0.5000	-0.5000	-37.7928	-37.2928
- - Angle xz	-12.0824	-0.0311	0.5000	-0.5000	-12.0513	-11.5513

Profile Esquerdo / Profile Direito:
Points 400
Filter type Low-pass Spline
Lc 0.25
Vmess[mm/sec] 3.00
Probe radius 1.2497
Evaluation method Nominal Vector Direction
Best Fit

	Translation	Rotation
X	0.0000	0.0000
Y	0.0000	0.0000
Z	0.0000	0.0000

Text
Event
-
n.def.

Figure A.6: Profile Measurement Report Blade 6

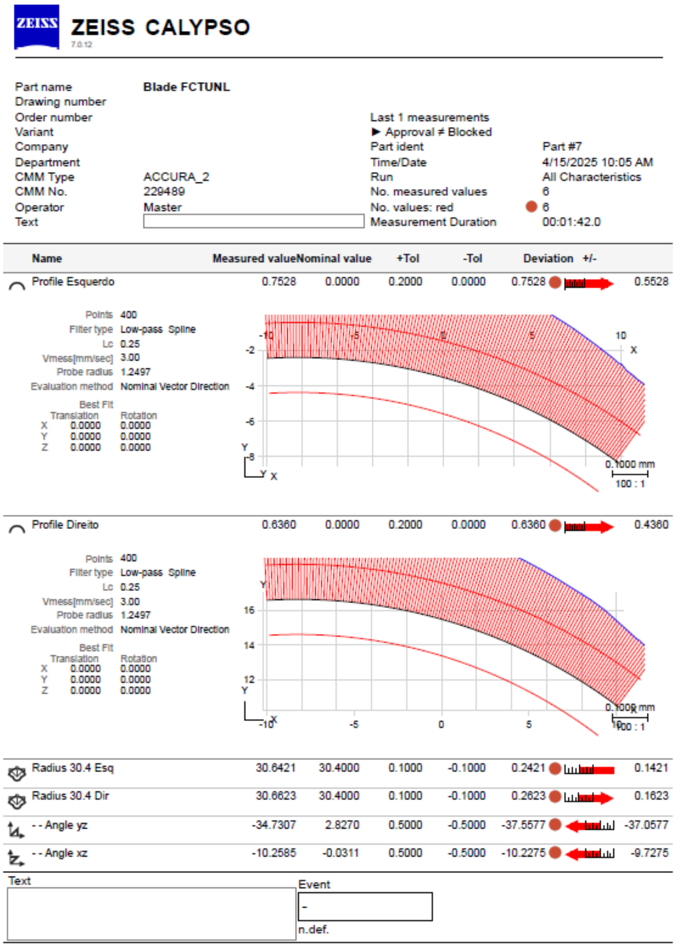

ZEISS CALYPSO

7.0.12

Part name	Blade FCTUNL		
Drawing number			
Order number		Last 1 measurements	
Variant		► Approval ≠ Blocked	
Company		Part ident	Part #7
Department		Time/Date	4/15/2025 10:05 AM
CMM Type	ACCURA_2	Run	All Characteristics
CMM No.	229489	No. measured values	6
Operator	Master	No. values: red	6
Text		Measurement Duration	00:01:42.0

Name	Measured value	Nominal value	+Tol	-Tol	Deviation	+/-
Profile Esquerdo	0.7528	0.0000	0.2000	0.0000	0.7528	0.5528
Profile Direito	0.6360	0.0000	0.2000	0.0000	0.6360	0.4360
Radius 30.4 Esq	30.6421	30.4000	0.1000	-0.1000	0.2421	0.1421
Radius 30.4 Dir	30.6623	30.4000	0.1000	-0.1000	0.2623	0.1623
- - Angle yz	-34.7307	2.8270	0.5000	-0.5000	-37.5577	-37.0577
- - Angle xz	-10.2585	-0.0311	0.5000	-0.5000	-10.2275	-9.7275

Profile parameters (both profiles): Points 400; Filter type Low-pass Spline; Lc 0.25; Vmess[mm/sec] 3.00; Probe radius 1.2497; Evaluation method Nominal Vector Direction; Best Fit Translation X 0.0000, Y 0.0000, Z 0.0000; Rotation 0.0000, 0.0000, 0.0000. Plot scale 0.1000 mm, 100 : 1.

Text

Event

-

n.def.

Figure A.7: Profile Measurement Report Blade 7

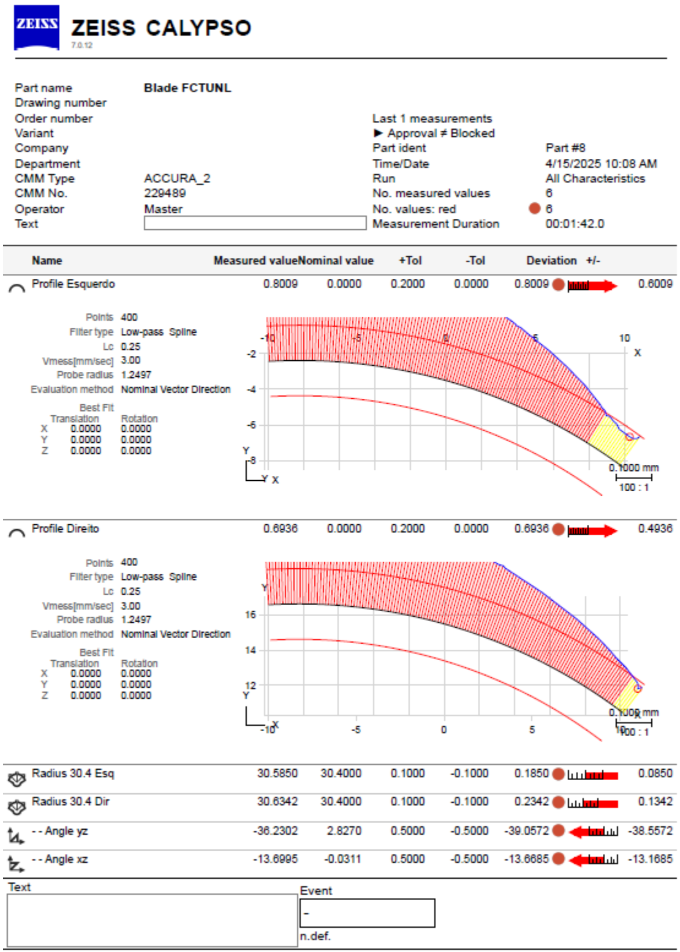

ZEISS CALYPSO

Part name	Blade FCTUNL		
Drawing number			
Order number		Last 1 measurements	
Variant		▶ Approval ≠ Blocked	
Company		Part ident	Part #8
Department		Time/Date	4/15/2025 10:08 AM
CMM Type	ACCURA_2	Run	All Characteristics
CMM No.	229489	No. measured values	6
Operator	Master	No. values: red	6
Text		Measurement Duration	00:01:42.0

Name	Measured value	Nominal value	+Tol	-Tol	Deviation	+/-
Profile Esquerdo	0.8009	0.0000	0.2000	0.0000	0.8009	0.6009
Profile Direito	0.6936	0.0000	0.2000	0.0000	0.6936	0.4936
Radius 30.4 Esq	30.5850	30.4000	0.1000	-0.1000	0.1850	0.0850
Radius 30.4 Dir	30.6342	30.4000	0.1000	-0.1000	0.2342	0.1342
- - Angle yz	-36.2302	2.8270	0.5000	-0.5000	-39.0572	-38.5572
- - Angle xz	-13.6995	-0.0311	0.5000	-0.5000	-13.6685	-13.1685

Profile Esquerdo / Profile Direito (same settings for both):

Points 400
Filter type Low-pass Spline
Lc 0.25
Vmess[mm/sec] 3.00
Probe radius 1.2497
Evaluation method Nominal Vector Direction

Best Fit

	Translation	Rotation
X	0.0000	0.0000
Y	0.0000	0.0000
Z	0.0000	0.0000

Text

Event
-
n.def.

Figure A.8: Profile Measurement Report Blade 8

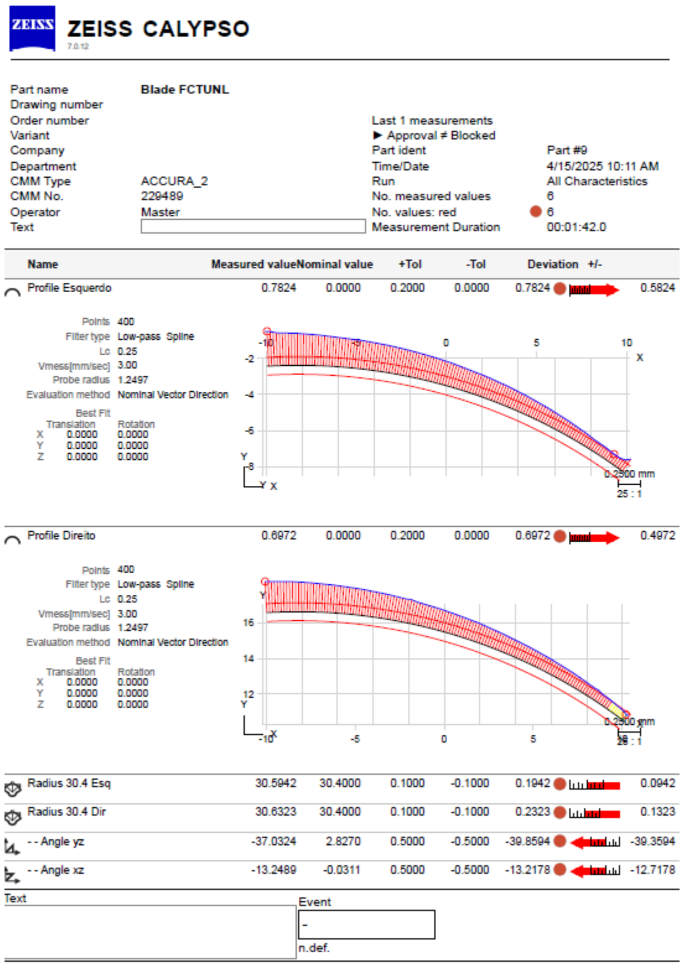

Figure A.9: Profile Measurement Report Blade 9

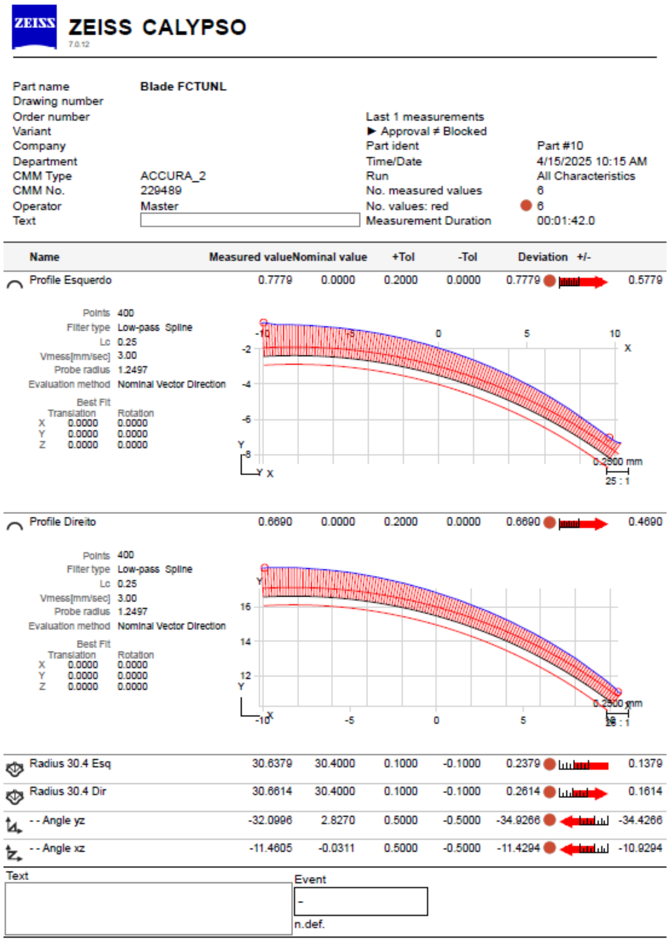

ZEISS CALYPSO

Part name	Blade FCTUNL		
Drawing number			
Order number		Last 1 measurements	
Variant		▶ Approval ≠ Blocked	
Company		Part ident	Part #10
Department		Time/Date	4/15/2025 10:15 AM
CMM Type	ACCURA_2	Run	All Characteristics
CMM No.	229489	No. measured values	6
Operator	Master	No. values: red	6
Text		Measurement Duration	00:01:42.0

Name	Measured value	Nominal value	+Tol	-Tol	Deviation	+/-
Profile Esquerdo	0.7779	0.0000	0.2000	0.0000	0.7779	0.5779
Profile Direito	0.6690	0.0000	0.2000	0.0000	0.6690	0.4690
Radius 30.4 Esq	30.6379	30.4000	0.1000	-0.1000	0.2379	0.1379
Radius 30.4 Dir	30.6614	30.4000	0.1000	-0.1000	0.2614	0.1614
- - Angle yz	-32.0996	2.8270	0.5000	-0.5000	-34.9266	-34.4266
- - Angle xz	-11.4605	-0.0311	0.5000	-0.5000	-11.4294	-10.9294

Profile parameters (both profiles): Points 400; Filter type Low-pass Spline; Lc 0.25; Vmess[mm/sec] 3.00; Probe radius 1.2497; Evaluation method Nominal Vector Direction; Best Fit Translation X 0.0000, Y 0.0000, Z 0.0000; Rotation 0.0000, 0.0000, 0.0000

Text | Event: - | n.def.

Figure A.10: Profile Measurement Report Blade 10

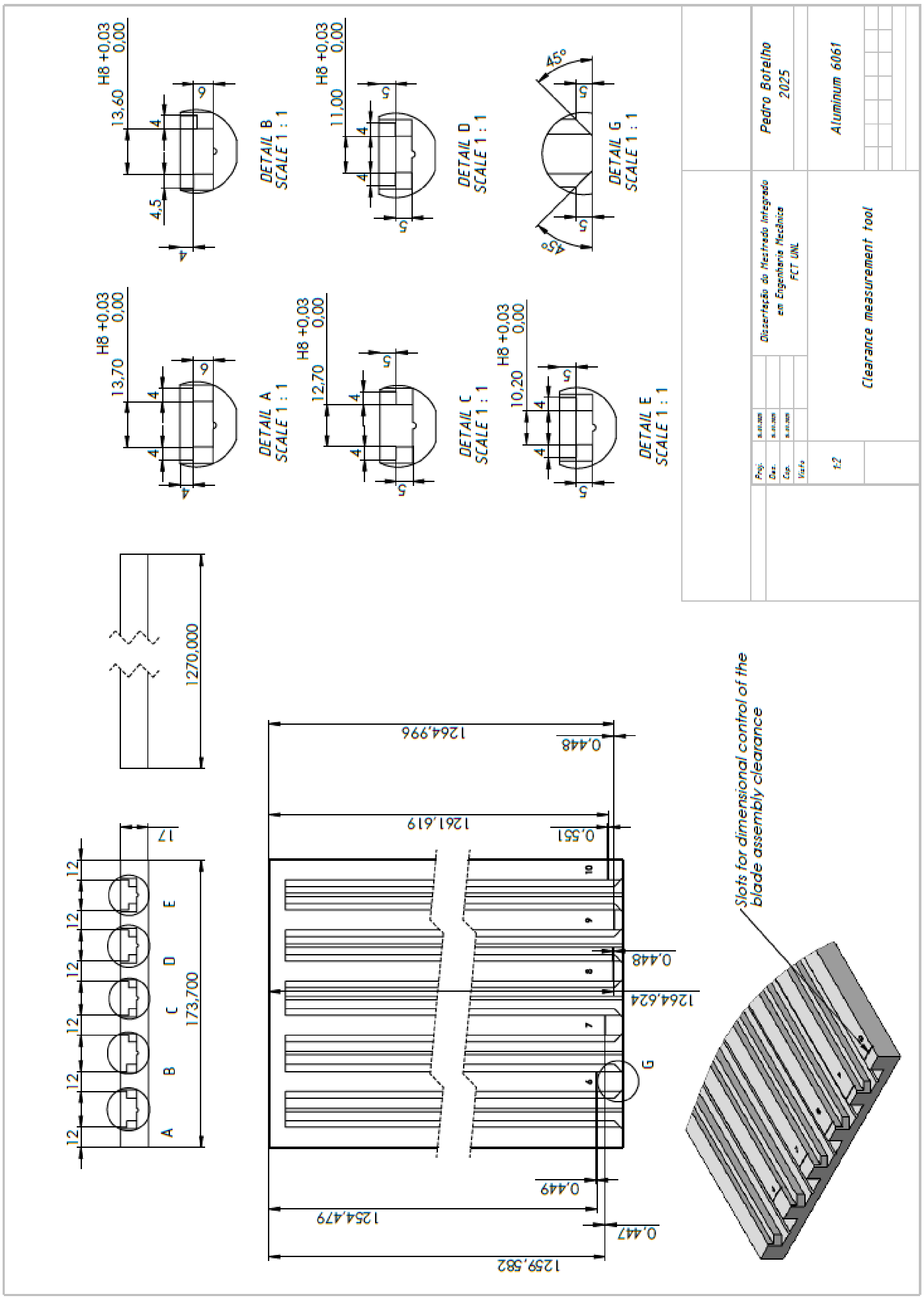

Figure A.11: First Tool Version 2D Drawing

⟨2025⟩ CONTROL AND OPTIMIZATION OF HIGH-PRESSURE COMPRESSOR BLADE DIMENSIONS AND CLEARANCES Pedro Botelho

NOVA SCHOOL OF SCIENCE & TECHNOLOGY